HHS Public Access

Author manuscript

Pain. Author manuscript; available in PMC 2022 November 01.

Published in final edited form as:

Pain. 2021 November 01; 162(11): 2750–2768. doi:10.1097/j.pain.0000000000002356.

Piezo2 mechanosensitive ion channel is located to sensory neurons and non-neuronal cells in rat peripheral sensory pathway: implications in pain

Seung Min Shin[1], **Francie Moehring**[2], **Brandon Itson-Zoske**[1], **Fan Fan**[3], **Cheryl L. Stucky**[2], **Quinn H. Hogan**[1,4], **Hongwei Yu**[1,4,*]

[1]Department of Anesthesiology, Medical College of Wisconsin, Milwaukee, WI 53226

[2]Department of Cell Biology, Neurobiology and Anatomy, Medical College of Wisconsin, Milwaukee, WI 53226

[3]Department of Pharmacology and Toxicology, Mississippi University Medical Center, Jackson, Mississippi 39216

[4]Zablocki Veterans Affairs Medical Center, Milwaukee, Wisconsin 53295

1. Introduction

Mechanosensitive ion channels are a diverse population of ion channels that integrate various internal and external mechanical cues to electrochemical mechanotransduction signals with different biophysical properties and biological significance [18, 33, 47, 57]. The evolutionarily conserved Piezo channels, including Piezo1 and Piezo2, are mechanically activated ion channels that play a critical role in a variety of mechanotransduction processes of different cell types [17, 51, 90]. Piezo1 mediates shear stress and stretch-induced transmembrane currents mainly in nonneuronal cells, whereas Piezo2 has been found predominantly expressed in primary sensory neurons (PSNs), where it confers proprioception and touch perception, and as shown more recently, detection of noxious mechanical stimuli [52]. In humans, mutations of genes expressing these channels are not life-threatening but result in different pathologies [13, 24]. Lack of painful reactions to innocuous touch after skin inflammation is reported in the loss-of-function mutations of *PIEZO2* but not *PIEZO1* [13, 54, 59, 78].

Various techniques have been employed to define Piezo2 expression in the PSNs of DRGs and trigeminal ganglia (TG), all of which detect Piezo2 expression in the PSNs. Initially, *in situ* hybridization (ISH) revealed Piezo2 expression in a subpopulation (20~60%) of large diameter low threshold mechanoreceptive (LTMR) PSNs in mouse DRG and trigeminal ganglia [4, 10, 17, 52, 56, 85, 87]. Similarly, single-cell RT-PCR using mouse DRG reports that *piezo2* mRNA is detected in 39% of all DRG-PSNs, including 26%, 33% and 60%

[*]**Correspondence author**: hyu@mcw.edu, phone: 414-955-5745.

Declaration of Competing Interest

The authors declare that they have no known competing financial interests or personal relationships that could have appeared to influence the work reported in this paper.

small-, medium-, and large-sized PSNs [61]. However, other studies also using ISH report that Piezo2 transcripts are expressed in all or most DRG-PSNs, including most notably the large-diameter neurons implicated in mediating touch and proprioception, as well as small-sized nociceptive PSNs [14, 46, 81, 98]. Immunohistochemistry (IHC) technique has observed Piezo2 expression in up to 45~80% of total PSNs of mouse DRG with high expression in large diameter PSNs [52, 73, 86], while a recent report describes Piezo2 expression in all PSNs of mouse DRG neurons, including large-diameter myelinated neurons encompassing LTMRs, as well as medium- and small-diameter nociceptors [80]. These reports of Piezo2 expression in ganglia are derived from mouse or duck [66], but Piezo2 expression has not been systematically examined in the rat peripheral nervous system (PNS).

Piezo2-knockout mice fail to develop allodynia after skin inflammation [73], while upregulation of Piezo2 activity correlates with inflammation-induced pain states, and inflammatory signals are found to enhance Piezo2-mediated mechanosensitive currents [21]. PSN-specific Piezo2 knockout mice develop less sensitization to noxious mechanical stimulation following spared nerve injury [52], suggesting Piezo2 participation in detection of such stimuli in inflammatory and neuropathic pain settings [30]. In order to pursue the therapeutic potentials targeting Piezo2 for chronic pain in preclinical rat models, this study was designed to characterize Piezo2 expression in the PNS of rats. We found that Piezo2 was expressed by all DRG neurons, a variety of non-neuronal cells in the peripheral sensory pathway, and spinal cord neurons. Presence of Piezo2 in spinal cord and peripheral glial cell populations suggests that Piezo2 may participate in sensory processing in spinal cord neurons and peripheral glial cells.

2. Methods

2.1. Animals

Adult male Sprague Dawley (SD) rats (6–8 week old, Charles River Laboratories, Wilmington, MA) were used. All animal experiments were performed with the approval of the Zablocki VA Medical Center Animal Studies Subcommittee and Medical College of Wisconsin Institutional Animal Care and Use Committee in accordance with the National Institutes of Health Guidelines for the Care and Use of Laboratory Animals. Animals were housed individually in a room maintained at constant temperature (22±0.5°C) and relative humidity (60±15%) with an alternating 12h light-dark cycle. Animals were given access to water and food *ad libitum* throughout the experiment, and all efforts were made to minimize suffering and the numbers of animals used. For tissue harvest euthanasia, animals were deeply anesthetized by isoflurane followed by decapitation with a well-maintained guillotine. The numbers of rats used are detailed in the relevant sections of the experiments. Piezo2 knockout (ko) mice (*Hoxb8Cre*/*Piezo2*$^{fl/fl}$) with C57BL/6J background at the age of ~6 month-old were generously provided by Dr. Ardem Patapoutian (Scripps Research Institute, CA). The keratinocyte-specific Piezo1-ko (*k14cre/Piezo1*$^{fl/fl}$) mice at the age of ~6 month-old were described previously [50].

2.2. Pain models

2.2.1. Intraplantar CFA inflammatory pain.—Inflammatory pain was induced by injection of a single dose of 100μl of CFA (Sigma-Aldrich, St. Louis, MO) at a concentration of 1.0 mg/ml or saline subcutaneously in the plantar surface of the right hind paw of isoflurane anesthetized rats, performed as described previously [27].

2.2.2. Mechanical allodynia and hyperalgesia: Mechanical allodynia was assessed as the mechanical withdrawal threshold (von Frey, vF) and hyperalgesia was identified by noxious punctate mechanical stimulation (Pin test), as described previously [23]. In brief, vF test was performed by applying the calibrated monofilaments (Patterson Medical, Bolingbrook, IL) to the plantar surface of the hindpaw. Beginning with the 2.8 g filament, if a response was observed, the next smaller filament was applied, and if no response was observed, the next larger was applied, until a reversal occurred, defined as a withdrawal after a previous lack of withdrawal, or vice versa. Following a reversal event, four more stimulations were performed following the same pattern. The forces of the filaments before and after the reversal, and the four filaments applied following the reversal, were used to calculate the 50% withdrawal threshold [23]. Rats not responding to any filament were assigned a score of 25 g. Pin test was performed using the point of a 22 g spinal anesthesia needle that was applied to the center of the hindpaw with enough force to indent the skin but not puncture it. Five applications were separated by at least 10s each, which was repeated after 2 min, making a total of 10 touches. For each application, the induced behavior was either a very brisk, simple withdrawal with immediate return of the foot to the cage floor, or a sustained elevation with grooming that included licking and chewing, and possibly shaking, which lasted at least 1s. This latter behavior was referred to as hyperalgesia behavior [88], which is specifically associated with place avoidance. Hyperalgesia was quantified by tabulating hyperalgesia responses as a percentage of total touches.

2.2.3. Tissue harvest for immunohistochemistry (IHC) and western blots.—Six naïve rats with normal mechanical sensory thresholds by vF and Pin tests were used for IHC characterization of Piezo2 expression. Specifically, lumbar (L) 4 and 5 DRG, trigeminal ganglia (TG), lumbar segment spinal cord, sciatic nerve trunk segment proximal to the sciatic bifurcation, brain, and hindpaw glabrous and hairy skin tissues; as well as lumbar spinal cord from CFA rats; and brain, lumbar spinal cord, L4/5 DRG, and hindpaw skin from mice; were dissected and fixed in Richard-Allan Scientific™ Buffered Zinc Formalin (ThermoFisher, Rockford, IL) overnight (~15 hr) for DRG, sciatic nerves, and skins; and 24 hr for spinal cord and brain; followed by processing for paraffin embedment. Serial sections at 5μm thickness; orientated at coronal for brain, sagittal for DRG and sciatic nerve, transverse for spinal cord, and perpendicular to the skin surface for glabrous and hair skin tissues; were prepared and mounted on the positive charged SuperForst microscope slides (ThermoFisher). For cryosection, fixed sciatic nerve tissues were cryoprotected by overnight infiltration with 30% sucrose solution in 1x phosphate-buffered saline (PBS), followed by mounting in OCT embedding compound, and freeze at −80 °C. Fifteen μm thickness cryosections were prepared on a crystate (Leica CM1950, Kyoto, Japan) and air-dried for 24 hr. For western blot experiments, L4/L5 DRG from CFA- and saline-injected rats, as well as

L3–5 DRG and lumbar spinal cord from mice, were dissected after cardiac perfusion with cold PBS, snap-frozen in liquid nitrogen, and stored at −80°C for extraction of protein.

2.3. Cell cultures

2.3.1. DRG dissociated culture and neuron-free SGC isolation [93, 95]: In brief, the L4/5 DRG were rapidly harvested from the isoflurane anesthetized naïve rats and were incubated in 0.01% blendzyme 2 (Roche Diagnostics, Madison, WI) for 30 min, followed by incubation in 0.25% trypsin and 0.125% DNase for 30 min; both dissolved in Dulbecco's modified Eagle's medium/F12 (DMEM/F12) with glutaMAX (ThermoFisher). After exposure to 0.1% trypsin inhibitor and centrifugation, the pellet was gently triturated and dissociated cells cultured in Neural basal media A (ThermoFisher) plus 0.5 μM glutamine at 37°C in humidified 95% air and 5% CO_2. Neuron-free SGC culture was established by a differential attachment protocol for SGC isolation, as we described previously [68].

2.3.2. Sciatic nerve (SN) Schwann cell isolation: The relevant steps required for nerve processing, enzymatic dissociation, and cell plating using the SN from one adult male rat was previously described, with minor modifications [5]. In brief, bilateral sciatic nerves were harvested and attached adipose and muscular tissue stripped off using fine forceps. Subsequently, the outermost epineurial layer and the epineurium were removed as one single sheath and collected for enzymatic digestion. The fibers were extensively teased until no individual fascicles were evident. The epineurium and teased fibers were subjected to digestion with an enzymatic cocktail for 4hr as described in DRG dissociated culture. The end products of enzymatic digestion were filtered and subsequently collected by centrifugation.

2.3.3. Cell lines: As a second source of Schwann cells, primary Schwann cells isolated from human spinal nerve were obtained from Neuromics (HMP303, Edina, MN). Primary adult human epidermal melanocytes were purchased from ThermoFisher (C0245C). Human SCs and isolated rat SCs were cultured in Schwann cell medium (Edina), and human epidermal melanocytes cultured in Medium 254 with melanocyte growth supplement (ThermoFisher), according to manufacturer's protocols. Neuronal cell lines of Neuro2A (N2A, mouse brain cortex neurons), F11 (rat DRG neuron-like cells), and Neuroblastoma B104 cells (B104) were obtained from ATCC (Manassas, VA), and rat DRG-neuronal 50B11 cells (50B11) were as prior reported [93], and these cells were cultured by a standard protocol at 37 °C with 5 % CO_2 in DMEM supplemented with 10% FBS and 1% penicillin-streptomycin (ThermoFisher).

2.4. Piezo2 knockdown and knockout (KD/KO) validation of Piezo2 antibody

For validation of Piezo2 antibody in a genetic strategy, the plasmids expressing of a short hairpin RNA against mouse Piezo2 in the coding region and a scrambled control (SC), in silico designed by use of BLOCK-iT RNAi Designer (Invitrogen), were generated. Specifically, a designed convergent U6 and H1 promoters driven apposing piezo2-shRNA (or SC) expression cassette was synthesized (Genscript, Piscataway, NJ) and cloned into Mlul site of an expression plasmid in which EGFP was transcribed by a CMV promoter.

These plasmids were named as pCMV-Piezo2shRNA-CMV-EGFP (pCMV-Piezo2shRNA) and pCMV-Piezo2SC-CMV-EGFP (pCMV-Piezo2SC), respectively. Transfection on N2A cells was performed by a standard PEI transfection protocol and Piezo2 knockdown efficacy determined by qPCR, western blot, and Piezo2 channel patch recording was performed 48hr post-transfection. Further Piezo2 antibody validation was performed on Piezo2-ko tissues by immunoblots and IHC. Piezo1 antibody was validated by IHC on skin sections of *k14cre/Piezo1*$^{fl/fl}$ mice.

2.5. RT-PCR and quantitative PCR (qPCR)

Total RNA was extracted from culture cells and DRG using RNAeasy kit (Qiagen, Carlsbad, CA, USA) and then treated with DNase I (Life Technologies). The concentration and purity of the total RNA were evaluated with a spectrophotometer. Complementary DNA (cDNA) was synthesized from 1.0 μg RNA using the Superscript III first strand synthesis kit with random hexamer primers (Life Technologies). PCR was carried out to determine Piezo2 mRNAs in 50B11 cells, DRG, isolated SGCs, isolated Schwann cells, and human melanocytes on a Bio-Rad C1000 PCR machine and specific intron-spanning primers from Piezo2 (and Piezo1) (Table 1). All of the primers were designed by use of MacVector version17.0.8 (https://www.macvector.com) and synthesized by Integrated DNA Technologies, Inc. (http://www.idtdna.com). The thermal cycling conditions were one cycle at 95°C for 3 min, 40 cycles at 95°C for 10 s, 60°C for 30 s, and 72°C for 50 s, followed by one cycle at 72°C for 5 min. A negative control with double-distilled water was performed for each PCR (and qPCR) experiment. QPCR was performed to determine Piezo2 knockdown effects by transfection of piezo2-shRNA into N2A cells using IQ Syber Green supermix (Bio-rad, Hercules, CA, USA) on a Bio-rad CFX96 Real-time PCR Machine and specific intron-spanning primers to quantify the cDNA levels of Piezo2 (Table 1). The thermal cycling conditions were one cycle at 95°C for 2 min, 40 cycles at 95°C for 10 s, 60°C for 10 s. The efficiency of the primers was 92–100% with r2>0.990. For each sample, two inter-run determinations were carried out, and two replicates in each run were averaged. For the comparative CT method, GAPDH was used as the housekeeping gene for calculation of fold differences in expression of Piezo2 mRNA. The relative amount of mRNA transcript in N2A cells transfected by Piezo2-shRNA to scrambled controls was measured by $2^{-\Delta\Delta C_t}$ calculation, where $\Delta\Delta C_t = (C_{t\ Piezo2} - C_{t\ Gapdh})_{control} - (C_{t\ Piezo2} - C_{t\ Gapdh})_{Piezo2shRNA}$.

2.6. Patch clamp recordings

For validation of Piezo2 functional knockdown, N2A cells transfected by pCMV-Piezo2shRNA or scrambled RNA (scrambled) were used for recording mechanically activated currents under the conventional whole-cell configuration. N2A cells were superfused continuously with RT extracellular normal HEPES solution containing (in mM): 140 NaCl, 5 KCl, 2 CaCl2,1 MgCl2, 10 HEPES, and 10 glucose, pH 7.4 ± 0.05, and 310 ± 3 mOsm, and viewed on a Nikon Eclipse TE200 inverted microscope. Cells were patch clamped in voltage clamp with a borosilicate glass pipette (Sutter Instrument Company, Novato, CA) filled with intracellular normal HEPES solution containing (in mM): 135 KCl, 10 NaCl, 1 MgCl2, 1 EGTA, 0.2 NaGTP, 2.5 ATPNa2, and 10 HEPES, pH 7.20 ± 0.05, and 290 ± 3 mOsm. Cell capacitance and series resistance were maintained below 10 MΩ. Mechanical stimulation was elicited using a second borosilicate glass pipette that was driven

by a piezo stack actuator (PA25, PiezoSystem Jena, Jena, Germany) at a speed of 106.25 μm/ms. Cells were stimulated with increasing displacements of 1.7 μm/Volt for 200 ms, and 2 min rest was allowed between displacements to avoid sensitization/desensitization of the cell membrane. Data was recorded using PatchMaster via an EPC10 amplifier HEKA Electronics, Holliston, MA). Data were analyzed using FitMaster (HEKA Electronics).

2.7. Immunofluorescent staining

2.7.1. Immunocytochemistry (ICC) and immunohistochemistry (IHC).—ICC on cultured human and isolated rat Schwann cells, human melanocytes, and DRG dissociated cultures, as well as IHC on tissue sections, were performed according to standard procedures [93]. For ICC, the cultured cells were fixed in 2% paraformaldehyde (PFA) in 1xPBS solution for 5 min; and for IHC, the formalin-fixed, paraffin-embedded (FFPE) tissue sections were deparaffinized, hydrated, and treated by heat-induced antigen epitope retrieval in 10mM citrate buffer, pH 6.0. Cryosections were treated by 3% hydrogen peroxide for 10 min to block endogenous peroxidase activity. Non-specific binding was reduced by incubating the sections for 30 min with a solution of 5% BSA in PBS plus 0.05% Tween20 (PBST) solution. Samples were first immunolabeled with the selected primary antibodies in a humid atmosphere overnight at 4°C (Table 2). All antibodies were diluted in PBST, containing 0.05% Triton X-100 and 5% bovine serum albumin (BSA). Normal immunoglobulin G (IgG from the same species as the first antibody, Table 2) was replaced for the first antibody as the negative controls. The appropriate fluorophore-conjugated (Alexa 488 or Alexa 594, 1:2000) secondary antibodies (Jackson ImmunoResearch, West Grove, PA) were used to reveal immune complexes. Afterward, the sections were rinsed for 10 min in PBS and either processed for a colabeling of primary and secondary antibodies or coverslipped under Shur/Mount mounting medium (ThermoFisher). To control for false-positive results attributable to cross-binding in double-label combinations, each primary antibody raised in a different species was used. To stain nuclei, 1.0μg/ml Hoechst33342 (Hoechst, ThermoFisher) was added to the secondary antibody mixture. The immunostaining was examined, and images captured using a Nikon TE2000-S fluorescence microscope (El Segundo, CA) with filters suitable for selectively detecting the green and red fluorescence using a QuantiFire digital camera (Optronics, Ontario, NY). For double label colocalization, images from the same specimen but showing different antigen signals were overlaid by digitally merging the captured images.

Two independently developed polyclonal Piezo2 antibodies, purchased from ProSci (Poway, CA) and Alomone (Jerusalem, Israel), were used. For control purposes (Piezo2 immunostaining), representative sections were processed in the same way as described but using nonimmune rabbit sera instead of the Piezo2 primary antibody in the incubation. We also tested the specificity by preincubating the antibody solution with the manufacturer's specific PIEZO2 antigenic peptides (2 μg/ml) for 2 hr prior to immunostaining, as described previously [79]. The specificities of the other antibodies used in this study have been previously confirmed, and the specificity of secondary antibodies was tested with omission of the primary antibodies, which always resulted in no immunostaining [79, 89, 93, 94].

2.7.2. Measurement and quantification of immunostaining—Positive marker antibody immunostainings were defined as the cells with the fluorescence intensity greater than average background fluorescence plus 2 standard deviations of the cells in an adjacent section in the same slide of negative control (the first antibody omitted) under identical acquisition parameters (n=10 for different markers), identified by Hoechst counterstain at a different wavelength [92]. For each comparative experiment, all images were acquired with identical settings for detector gain and exposure time under a 10x objective (0.5 numerical aperture at 2048×2048 pixel resolution) or 20x objective (0.3 numerical aperture at 1024×1024 pixel resolution).

Intensity correlation analysis (ICA) was performed to determine colocalization of Piezo2 with neuronal plasma membrane (PM) marker sodium/potassium ATPase 1 alpha (NKA1a) and SGC marker glial fibrillary acidic protein (GFAP) in rat, as previously described using an ImageJ 1.46r software plugin colocalization analysis module (http://imagej.nih.gov/ij) [40, 68, 95]. In brief, fluorescence intensity was quantified in matched region of interests (the green and red colors varied in close synchrony) for each pair of images. The mean background was determined from areas outside the section regions and was subtracted from each file. On the basis of the algorithm, in an image where the intensities vary together, the product of the differences from the mean (PDM) will be positive. If the pixel intensities vary asynchronously (the channels are segregated), then most of the PDM will be negative. The intensity correlation quotient (ICQ) is based on the nonparametric sign-test analysis of the PDM values and is equal to the ratio of the number of positive PDM values to the total number of pixel values. The ICQ values are distributed between −0.5 and +0.5 by subtracting 0.5 from this ratio. In random staining, the ICQ approximates 0. In segregated staining, ICQ is less than 0, while for dependent staining, ICQ is greater than 0.

Lumbar spinal cord sections from control rats and from rats subjected to CFA inflammatory pain, as well as archival spinal cord sections from neuropathic pain models of SNL, SNI, and TNI (4wk post injury), and MIA-OA pain (5wk after MIA knee injection), as previously reported [42, 67–69, 95, 96], were used to evaluate whether pain is associated with alteration of Piezo2 expression in the DH. For quantification of DH piezo2 immunostaining, the Image J v.1.46 was used to quantify changes in immunolabeled fluorescent intensities as described previously [16, 67], with some minor modifications. In brief, the sections with symmetrical width of DH throughout the mediolateral axis were used for measurement, and the upper and lower threshold optical intensities were adjusted to encompass and match the immunoreactivity (IR) that appears in red. A standardized rectangle was first positioned over laminae territory throughout the mediolateral axis on the contralateral DH. The area and intensity of pixels within the threshold value representing IR were calculated and the integrated intensity was the product of the area and density. The same box was then moved to the corresponding position on the opposite DH and the integrated intensity of pixels within the same threshold was again calculated. Comparisons of both sides of DHs were made only within the same sections and intensity values on the ipsilateral side were expressed as a percent of the contralateral side, providing an estimate of fold change (ratio of ipsilateral/contralateral) for each section.

2.8. Immunoblot analysis of Piezo2 expression

Cell and tissue lysates were prepared from Neuro2A, F11, B104, 50B11 cells, and DRG. The collected cell pellets and pooled L4/L5 DRG from CFA and control rats, as well as pooled L3–L5 DRG and lumbar spinal cord from wild-type and Piezo2-ko mice, were extracted using 1x RIPA ice-cold buffer (20 mm Tris-HCl pH 7.4, 150 mm NaCl, 1% Nonidet P-40, 1% sodium deoxycholate, 0.1% SDS, with 0.1% Triton X100 and protease inhibitor cocktail) and rotated at 4 °C for 1 h before the supernatant was extracted by centrifugation at 12,000 g at 4 °C for 5 min. To examine the subcellular localization of Piezo2, rat DRG tissues were homogenized and then fractionated to obtain plasma membrane and cytosolic fractions, using the ProteoExtract Subcellular Proteome Extraction Kit (Millipore, Billerica, MA), according to the manufacturer's instructions. This kit contains extraction buffers with ultrapure chemicals to ensure high reproducibility, protease inhibitor cocktail to prevent protein degradation, and benzonase nuclease to remove contaminating nucleic acids. Protein concentration was determined using Pierce BCA kit (ThermoFisher). Equivalent protein samples (cell lysates and DRG membrane and cytosol) were size separated using 10% or 4–20% SDS-PAGE gels (Bio-Rad), transferred to Immun-Blot PVDF membranes (Bio-Rad), and blocked for 1 hr in 5% skim milk. In some experiments, the transferred PVDF membranes were cut into two halves along protein size around 70KDa and were subsequently incubated overnight at 4°C with appropriate antibodies. Immunoreactive proteins were detected by Pierce enhanced chemiluminescence (ThermoFisher) on a ChemiDoc Imaging system (Bio-Rad) after incubation for 1 hr with HRP-conjugated second antibodies (1:5000, Bio-Rad). Between each step, the immunoblots were rinsed with Tris-buffered saline containing 0.02% Tween-20 (TBST). To verify the band specificity of Piezo2 detection using a rabbit Piezo2 antibody, the antibody solution was preincubated with the manufacture's specific Piezo2 antigenic peptides (2 μg/ml) for 2 hr prior to immunoblotting.

2.9. Statistics

Statistical analysis was performed with GraphPad PRISM 8 (GraphPad Software, San Diego, CA). Significances of ICQs of Piezo2 immunocolocalization with NKA1α and GFAP were analyzed by means of the normal approximation of the nonparametric Wilcoxon rank test, as described previously [40, 95]. Mechanical allodynia and hyperalgesia were compared between groups by Student's *t*-test for von Frey and by Mann–Whitney test for Pin. Patch recordings were analyzed using a repeated measures two-way ANOVA with Sidak *post-hoc* comparison. The differences of the targeted gene expression by qPCR, immunoblots, and DH Piezo2-IR intensity analysis on the spinal cord sections between different groups were compared with 2-tailed unpaired Student's t test or Mann–Whitney test where appropriate. Results are reported as mean and SEM. $P<0.05$ were considered statistically significant.

3. Results

3.1. Specificity determination of Piezo2 antibody

Since the specificity and sensitivity for detection of Piezo2 expression is largely dependent on the quality of the first antibody, we decided to use two different, independently developed

Piezo2 antibodies to optimize immunological detection of Piezo2 for ensuring specific detection of the Piezo2 protein expression in the cultured cells and DRG tissue. These two Piezo2 antibodies were chosen because the manufacturer's western blot data show detection of protein bands with molecular mass of putative canonical Piezo2 and its isoforms (GenBank and ExPASy database), as well as the antigenic peptides are available. The first Piezo2 antibody was purchased from ProSci (Fort Collins, CO), which is an affinity chromatography purified rabbit polyclonal antibody raised against an intracellular peptide corresponding to 19 amino acids (HLTASLEKPEVRKLAEPGE, 14/19 homologous to rat sequence) near the amino terminus of human PIEZO2 (NP_071351), and predicted detection of PIEZO2 proteins of 233 and 305 KDa by immunoblot, no cross-reaction to Piezo1, and signals are blocked by antigenic peptide preabsorption. The second Piezo2 antibody, obtained from Alomone (Jerusalem, Israel), is also a rabbit polyclonal antibody which is raised, and affinity purified on immobilized antigenic peptide (RTIFHDITRLHLD, 12/13 homologous to rat sequence) corresponding to 13 amino acid residues (1092 −1104) of human PIEZO2. Manufacturer's in-house data show that this antibody detects Piezo2 expression in rat DRG lysates of ~300 and ~180 kDa by immunoblot and signals are blocked by antigenic peptide preabsorption. The antigenic peptide sequences of these two antibodies are located in the predicted intracellular loop regions of human Piezo2 [82].

An initial experiment was performed to characterize Piezo2 detection in the lysates prepared from several neuronal cell lines and from DRG of naïve rat by use of Piezo2 antibody from ProSci. The canonical Piezo2 is composed of ~2800 amino acids with a molecular mass at ~310KDa and predicted to be modified by phosphorylation and glycosylation. Also, PSN *Piezo2* has been found to undergoes differential gene splicing, resulting in many alternatively spliced and different functional Piezo2 mRNAs that may be translated to different molecular weight (MW) protein isoforms [7, 74]. Seven or eight potential Piezo2 protein isoforms are computationally mapped in human and mouse (https://www.uniprot.org); but whether they are the biological products derived from gene alternative splicing or canonical Piezo2 proteolytic processing are remained to be established. Multiple bands in the range of 310–150kDa were noted upon immunoblotting in the homogenates of neuronal cell lines, all of which were eliminated by preincubation with excess (2μg) manufacturer's immunogenic peptide (Fig. 1A). In rat DRG lysate, the antibody detected several bands with predicted molecular masses approximately at 310, 240, 180, and 130 kDa, and they were all eliminated by preincubation with immunogenic peptide (Fig. 1B). To verify membrane localization, we performed Piezo2 immunoblots in the cytosolic and membrane fractions prepared from the DRG harvested from naïve rats and results showed that the antibody detected protein bands of ~240kDa and ~180kDa that were more enriched in membranes while the protein bands with kDa at ~310 and ~130 were more enriched in cytosolic fractions (Fig. 1C).

IHC revealed a pan-neuronal pattern of Piezo2-IR in rat DRG section and preincubation with Piezo2-specific antigenic peptide eliminated IHC staining (Fig.1D, D1). This effect was not observed when IHC was performed by preincubating Piezo2 antibody with a non-specific ($Ca_V3.2$) antigenic peptide (Alomone; not shown), which provides additional validation for the selectivity. A pan-neuronal pattern of Piezo2-IR was also identified in the rat TG (Fig. 1E). Similar findings were confirmed using the second independent Piezo2 antibody

(Alomone) by immunoblot and IHC on DRG tissues, but this antibody seemed somewhat less sensitive for detecting Piezo2 by IHC. IHC using Alomone Piezo2 antibody on sections from TG sections also showed a pan-neuronal pattern of Piezo2 expression (see below).

Selectivity of the ProSci Piezo2 antibody was further validated by comparing the relevant immunoblot Piezo2 protein level in the control N2A cells versus the N2A cells in which the RNAi induced Piezo2 knockdown, as was verified by qPCR and patch-recording of Piezo2 channel activity. As shown in Fig. 1F–I, shRNA-mediated knockdown of Piezo2 reduced the Piezo2-antibody recognized bands (~310kDa and ~250kDa) but no significant reduction of protein bands with kDa at ~180 and ~130 (not shown), compared to the bands in the scrambled control-transfected cells, and these results correlate with an equivalent reduction of Piezo2 mRNA by qPCR quantification (approximately 80% for both; ~310kDa and ~250kDa bands in western blots were combined for calculation). In parallel, shRNA knockdown reduced mechanically-evoked rapid-adapting whole-cell current (Fig. 1J, K). Besides the above approaches, the Piezo2 antibody specificity was also analyzed using DRG, spinal cord, and skin collected from Piezo2-ko mice (*Hoxb8Cre*/*Piezo2*$^{fl/fl}$ in which *Hoxb8Cre* induces floxed *Piezo2* deletion) [52, 84]. Hindlimb coordination defects were observed in *Hoxb8Cre*/*Piezo2*$^{fl/fl}$ mice as reported [86]. As shown in Fig. 2, Piezo2 protein that displayed a strong ~300kDa band upon immunoblot of DRG and lumbar spinal cord lysates in wild-type mice was barely detected in Piezo2-ko mice. Piezo2 ablation did not affect Piezo1 expression as there were no differences of Piezo1 protein expression in both DRG and spinal cord between wild-type and Piezo2-ko DRG lysates by immunoblots using a cell-based-KD [72] and *C14Cre/Piezo1*$^{fl/fl}$-KO (Suppl. Fig. 1) validated Piezo1 antibody. Piezo2-IR in the DRG from wild-type mice was detected in all PSNs by IHC, whereas Piezo2-IR was minimally detectable in Piezo2-ko mice. Consistent with the rat IHC data (see below in Fig. 3), Piezo2-IR was detected in the spinal cord showing a neuronal profile, but Piezo2-IR was minimally detected in Piezo2-ko mice. Additionally, keratinocyte Piezo2-IR in Piezo2-ko mice was also apparently decreased compared to wild-type mice. These data provide evidence supporting the specificity of ProSci Piezo2 antibody. Based on these findings, the ProSci Piezo2 antibody was used for further IHC and immunoblot experiments, unless stated otherwise.

3.2. Piezo2 expression in the rat PNS

3.2.1. Neuronal and glial Piezo2 expression in DRG (Fig. 3): We next determined the Piezo2 expression within rat DRG sections by double immunolabeling using Piezo2 antibody with various established and distinct neuronal markers including Tubb3 (pan neurons), nonpeptidergic IB4-biotin (nonpeptidergic small neurons), peptidergic CGRP (peptidergic neurons), NKA1α (neuronal plasma membrane), NF200 for large Aβ low-threshold mechanoreceptors (Aβ-LTMRs) and proprioceptors, and TrkB (Aδ-LTMRs) [39, 63, 98]. We found Piezo2-IR in all Tubb3-positive PSNs, suggesting pan-neuronal expression of Piezo2 in rat DRG, a finding that is consistent with the recent results from RNAscope ISH and IHC [80, 81, 98]. All IB4- and CGRP-positive neurons which consist of 45% and 59% of Piezo2-positive neurons, respectively, were Piezo2 immunopositive, indicating that Piezo2 is highly expressed by unmyelinated (C-type) and thinly myelinated (Aδ-type) PSNs that convey the thermal and mechanoreceptive nociceptive signals generated

at peripheral nerve terminals to neurons in lamina I-II of the spinal cord [20]. Nociceptive neurons in adult rat DRG can be double positive for both IB4 and CGRP (30–40%) [95], suggesting that there is a substantial proportion of small Piezo2-IR neurons positive for both IB4/CGRP. Colabeling of Piezo2 with NKA1α revealed enriched Piezo2 profiles in the PSN plasma membrane, especially those of larger diameter neurons. Nearly all NF200-neurons that consist of 30% among Piezo2-IR neurons were Piezo2 immunopositive, suggesting detection of Piezo2 expression in the Aβ-LTMRs and proprioceptive PSNs that transmit mechanoreceptive and proprioceptive signals via thickly myelinated afferents (Aβ-type) to spinal lamina III-V. Most of Piezo2-positive PSNs were also positive for TrkB, suggesting high expression of Piezo2 in the Aδ-LTMR neurons (Fig. 3A–F1). To obtain further insight into plasma membrane (PM) localization of Piezo2, we examined the ICA of the images co-stained Piezo2 with NKA1α. Overlaid images of Piezo2 with NKA1α showed colocalizations of the two patterns of immunopositivity (Fig. 3F1), but the ICA plots of Piezo2 and NKA1α resulted, however, in a more complex relationship in which the data tended to cluster along both positive and negative axes with ICQ 0.04–0.2 (p <0.01~ 0.001, n=10), indicating partial localization of Piezo2 in neuronal PM (**G**). ICC on DRG dissociated culture also identified Piezo2 expression in the neurons, as well as S100- and GFAP-positive glial cells (Suppl. Fig. 2).

Next, we performed IHC using various established glial cell markers for the satellite glial cells (SGCs) and Schwann cells (SCs), including glutamine synthetase (GS), glial fibrillary acidic protein (GFAP), S100, and myelin basic protein (MBP) [68]. This was performed in order to rule out Piezo2 expression in the perineuronal glial cells, which produce ring-like immunopositivity that resembles NKA1α staining patterns. Unexpectedly, IHC staining revealed Piezo2-IR in the S100-, GFAP-, and GS-positive perisomatic glial population, indicating Piezo2 expression in SGCs and/or SCs (Fig. 3H–L1) since both express those glial markers [64]. This could be expected on the basis that SGCs may represent a population of developmentally arrested Schwann cells [26]. To further verify the Piezo2 expression in the perineuronal glia, ICA was performed to analyze the immunocolocalization between Piezo2 and GFAP. Overlaid images of Piezo2 with GFAP showed colocalizations of two immunopositivity (Fig. 3L1), and the ICA plots of Piezo2 and GFAP also clustered along both positive and negative axes with ICQ 0.06–0.26 (p < 0.01~0.001, n=10), indicating Piezo2 partial colocalization in perineuronal glia cells (Fig. 3M). No apparent co-labeling was observed between Piezo2 and MBP which is a major constituent of periaxonal myelin laminae and a myelinating Schwann cells (mySCs) marker. This suggested that Piezo2 was expressed by non-myelinating SCs (nmSCs) but not mySCs (Fig. 3J). A search of deposited microarray data in the GenBank GEO Profile corroborated our finding since Piezo2 transcripts, as well as Piezo1 transcripts, have been detected in the cultured human Schwann cells (https://www.ncbi.nlm.nih.gov/geoprofiles/?term=Piezo2+schwann) and SGCs in a recent publication [31]. This provides support for our finding that Schwann cells express Piezo2.

3.2.2. Detection of Piezo2-IR in sciatic nerve, spinal cord, and skin: We next characterized Piezo2 expression in the DRG-PSNs innervating tissues in rats. Results showed that high Piezo2 immunostaining signals were detected in the sciatic nerve, which

co-stained with neuronal markers of Tubb3, NF200, IB4, and CGRP (Fig. 4A–D), indicating that Piezo2 was actively transported along the afferent axons, including myelinated fibers and C/Aδ fibers. Notably, sciatic nerve Piezo2 immunostaining displayed Schwann cell components since Piezo2 signals were colocalized to Schwann cell markers of S100, p75NTR, GFAP, and, to a less extent, MBP (Fig. 4E–H). ICC colabeling of Piezo2 with S100 on human SCs and isolated SCs from rat sciatic nerve verified Piezo2 expression in SCs (Fig. 4I, J).

The spinal cord DH is a key site for integrating and transmitting somatosensory information [2, 36]. GenBank GEO Profile shows detection of both Piezo2 and Piezo1 transcripts in spinal cord by microarray (https://www.ncbi.nlm.nih.gov/geoprofiles) and RNAseq, including dorsal horn and motor neurons [11, 19, 29, 34, 45, 83, 91, 97]; enriched Piezo2 is detected in human induced pluripotent stem cell (iPSC)-derived spinal motor neurons [43]; and the HUMAN PROTEIN ATLAS shows consensus datasets of enhanced Piezo2 transcript detection in spinal cord (https://www.proteinatlas.org/ENSG00000154864-PIEZO2/tissue). These data provide credent evidence of Piezo2 in spinal cord neuronal transcriptome, but Piezo2 channel protein expression in the spinal cord has not been fully defined [53]. Since IHC revealed actively axonal transporting of Piezo2 to peripheral afferents (Fig. 4), we examined whether Piezo2 was also transported to the central terminals innervating the DH. IHC on rat lumbar spinal cord sections revealed extensive Piezo2-IR in the intrinsic spinal cord neurons of both the DH and the ventral horn (VH). Colabeling of Piezo2 with NeuN verified that Piezo2 was expressed in the spinal cord postsynaptic neurons, including DH interneurons and VH motor neurons (Fig. 5A, B). Indeed, Piezo2-IR signals were present in the central terminals of peptidergic and nonpeptidergic neuropil that synapse in the DH of the spinal cord. These are likely transported along axons from DRG-PSNs since DH Piezo2-IR was highly overlaid to presynaptic markers of IB4, CGRP, synaptic vesicle protein synaptophysin (Syp), and synaptoporin (Synpr) (Fig. 5C–F) [94]. DH Piezo2-IR did not present in GFAP-positive astrocytes and Iba1-positive microglia (Fig. 5G, H). Finally, Piezo2 was also extensively detected in the brain neurons (Suppl. Fig. 3), a finding in agreement with a recent report that shows Piezo2 expression in mouse brain neurons using an independent Piezo2 antibody raised by a Piezo2 C-terminal peptide [80].

Skin Merkel cells express Piezo2, functioning for Merkel-cell mechanotransduction [22, 25, 87]. We also found Piezo2-IR in the Merkel cells of the hindpaw epidermis, which colabeled with CK14, a marker for the basal keratinocytes and Merkel cells (Fig. 6A, A1, B) [44, 87]. Data also displayed Piezo2-IR in Meissner's corpuscles (Fig. 6B) [25], the afferent terminal nerve bundles in dermis (Fig. 6C–H), and lanceolate endings around hair follicles (Fig. 6I, J) [58]. Piezo2-IR in the epidermal basal layer keratinocytes was colabeled with S100, which is a well-validated melanocyte (or pigment cells) marker but is negative for Merkel cells (Fig. 6K, K1) [55]. Additionally, S100-IR was overlaid to the Piezo2-IR signals in Meissner's corpuscles and Schwann cells surrounding cutaneous afferent nerve bundles within dermis, suggesting that Piezo2 was likely expressed by cutaneous Schwann cells (Fig. 6H, K, K1, L). Co-labeling of Piezo2 with S100 by ICC on the cultured human epidermal melanocytes verified piezo2 expression in the melanocytes (Fig. 6M–P). This indicates that Piezo2 is not restricted to the Merkel cells and epidermal melanocytes also express Piezo2.

3.2.3. Confirmation of Piezo2 expression by RT-PCR.—

RT-PCR was performed on the total RNAs extracted from 50B11 cells (rat DRG neuronal cells), rat DRG tissue, primary cultured SGCs and Schwann cells prepared from naïve rats, and primary cultured human melanocytes. Results showed amplification of Piezo2 (and Piezo1) transcripts by use of two different pairs of primers specific for Piezo2 (and Piezo1) in these samples, indicating that Piezo2 was expressed in DRG (PSNs), SGCs, Schwann cells, and human melanocytes (Fig. 7).

3.2.4. Confirmation with a second Piezo2 antibody.—

Immunoblots and IHC of Piezo2 protein expression in DRG comparing wild-type and Piezo2-ko mice validated the specificity of an alternate Piezo2 polyclonal antibody (Alomone) and verified that this antibody may also be useful in IHC experiments to detected Piezo2-IR in neurons and non-neuronal cells of PNS (Suppl. Fig. 4). IHC of rat tissues using this alternate Piezo2 polyclonal antibody showed a similar profile of Piezo2 immunopositivity in DRG- and TG-PSNs and perineuronal glia, sciatic nerve Schwann cells, Meissner's corpuscles, lanceolate endings around hair follicles, and epidermal Merkel cells and melanocytes (Suppl. Fig. 5). The observed similarity of patterns in both immunoblots and IHC results between two independent Piezo2 antibodies support the validity of our experimental findings.

3.3. Elevated Piezo2 expression in rat CFA-induced inflammatory pain.

Previous studies in humans and mice indicate that Piezo2 is an essential mediator of touch under inflammatory conditions, and inflammatory signals enhance piezo2-mediated mechanosensitivity [21, 73]. We next attempted to determine whether inflammatory pain was associated with alteration of Piezo2 protein expression in DRG and spinal cord. We generated CFA inflammatory pain, confirmed by reduced the threshold for withdrawal from mild mechanical stimulation (von Frey) and hyperalgesia evident with noxious (Pin) mechanical stimulation (Fig. 8A) when compared to baseline or CFA rats receiving only saline injection. L4/L5 DRG and lumbar spinal cords were harvested at the 10-day after CFA for western blots (DRG) and IHC (spinal cord). To evaluate the protein expression level of Piezo2 located in the DRG and intracellular trafficking alteration, we separately examined Piezo2 protein levels in the NKA1α-enriched membrane fractions versus the NKA1α-deficient cytosolic fractions. Multiple bands were noted upon immunoblotting and canonical Piezo2 (~310KDa) and ~250-KDa bands, which were clearly separated, were significantly increased in both membrane and cytosols from the DRG ipsilateral to CFA injection, compared to controls (Fig. 8B, C).

Since the spinal cord DH receives innervation from DRG-PSNs, we next evaluated by IHC whether CFA pain was associated with altered Piezo2 expression in the DH. For quantitative comparison, we normalized Piezo2-IR intensity on the side ipsilateral to CFA by using the contralateral side in the same section as the control [16, 67], assuring that all IHC preparation and image capture parameters are identical in the same cross-section. To validate the use of general IR intensity of the DH as a quantitative indicator of protein expression in sensory neurons, we compared IB4 and CGRP staining in the DH from SNI rats, in which quantitatively decreased IB4 and CGRP immunoreactive intensity in sensory neurons ipsilateral to the SNI injury is expected [42, 95]. As shown in Suppl. Fig. 6,

control rats showed symmetrical patterns of IB4 and CGRP staining in the superficial DH neuropil, whereas 4-week after SNI, quantitative evaluation revealed ipsilateral IB4 and CGRP IR intensity down to 50±4% and 15±3% of contralateral controls, respectively. We next performed Piezo2 IHC on the sections prepared from saline- and CFA-injected rats, and quantitative analysis of the Piezo2-IR intensity ratio between ipsilateral to contralateral DH revealed an enhanced Piezo2-IR in the ipsilateral side compared to the contralateral side in CFA animals (Fig. 8D–F).

3.4. Increased DH Piezo2-IR intensity in multiple pain conditions in rat

To provide insight into whether DH Piezo2 is also elevated in other pain models, we examined previously archived FFPE axial sections of the lumbar spinal cords from control rats and from rats subjected to neuropathic pain models of SNL, SNI, and TNI (4wk post injury) [42, 67–69, 95, 96], as well as MIA-OA pain (5wk after MIA knee injection), at which time the animals had developed typical hypersensitivity to mechanical stimuli (Fig. 9A–D). Results showed that DH Piezo2, determined as the ratio of intensity of IR on the ipsilateral side divided by the contralateral side, was significantly increased in SNL, SNI, and TNI, as well as MIA (Fig. 9E–M). These data suggest that DH Piezo2 protein levels are increased in a wide variety of pain models.

4. Discussion

We present data here showing that Piezo2 is extensively expressed in the sensory neurons and non-neuronal cells in rat peripheral sensory pathways. The major findings include: 1) Piezo2 is expressed by majority of DRG-PSNs, consistent with the recent reports by ISH or IHC showing Piezo2 expression in the majority of DRG-PSNs of mice [80, 81, 98]; 2) Location of Piezo2 expression extends from peripheral terminals in the skin to central presynaptic terminals in the spinal DH; 3) At least two putative Piezo2 isoforms are likely present in DRG, although further biological validation remains to be established; 4) Piezo2 is additionally expressed by DH postsynaptic neurons, motor neurons, and brain neurons; 5) Piezo2 is detected in peripheral non-neuronal cells, including perineuronal glia which are composed of SGCs and nmSCs, sciatic nerve and cutaneous SCs, and skin epidermal melanocytes, as well as Merkel cells; and 6) Spinal DH Piezo2-IR intensity, an indicator of protein levels, was significantly increased in multiple pain conditions, including CFA inflammatory pain, neuropathic pain, and MIA-OA pain. These observations indicate that Piezo2 function related to sensation may involve intimate and sophisticated interactions of PNS neuron-glia and axon-SCs, as well as presynaptic and postsynaptic sensory circuits in the spinal cord.

Piezo2 has emerged as a target of considerable interest in pain research and has mostly been studied in PSNs and Merkel cell biology, touch sensation, and innoxious mechanical pain [6]. However, a consensus is not yet established regarding its role in pain pathogenesis. For example, Piezo2 is persuasively described as a LTMR touch receptor expressed in large PSNs, but new studies indicate that the majority of DRG-PSNs express Piezo2, including IB4 non-peptidergic nociceptors which contain the population of neurons specifically mediating mechanical pain response and CGRP neurons which have been

proposed to mainly mediate noxious heat response [71]. Mice PSN-selective Pizeo2 deletion develop tactile allodynia, while other study reports that PSN-selective Piezo2 knockout in mice impairs touch but sensitizes mechanical sensitivity [98]. Piezo2 may also integrate mechanical and thermal cues in vertebrate mechanoreceptors [99]. Function of Piezo2 in pain has been interpreted based on the early experimental data showing that PSNs express only Piezo2 but absent in Piezo1; however, recent studies show that functional Piezo1 is also expressed in PSNs [48, 61, 98]. The Piezo isoforms are not known to form Piezo1-Piezo2 hybrid, but co-expression of Piezo1 and Piezo2 in sensory neurons raises an interesting issue of potential functional interactions between these channels. The apparent similarity in functional properties suggests the possibility of Piezo1 and Piezo2 to cooperate via synergistic or negative interaction [38, 99] or provide redundancy for each other [81] in mechanotransduction and pain pathogenesis.

Detection of Piezo2 protein expression in the spinal cord has not been described previously [53], although credent Piezo2 transcript detection in spinal cord has been reported [97]. Our new data show that Piezo2 expression in PSNs extends from peripheral terminals in the skin to central presynaptic terminals in the DH. Additionally, Piezo2 is abundantly expressed by somata of spinal cord neurons, including superficial and deeper DH neurons and ventral horn motor neurons. Somatosensory information is transmitted from primary afferent fibers in the periphery into the central nervous system via the DH that functions as an intermediary processing center for this information. In general, innocuous touch transmitted by Aβ-LTMR afferents projects to the deep DH LTMR recipient zone (LTMR-RZ) and synapse with interneurons in the deeper DH laminae, while noxious afferents and high threshold mechanoreceptors (HTMRs) terminate predominantly in laminae I–II [2]. Therefore, Piezo2 may play unexplored roles in normal and possibly pain sensory processing of spinal cord. Importantly, we found that the DH Piezo2-IR intensity, an indicator of protein levels, was significantly increased in multiple pain conditions, including neuropathic pain, CFA inflammatory pain, and MIA-OA pain. This may imply the redistributed and upregulated PSN-Piezo2 in the DH central terminals, as have been reported that some pronociceptive channels, such as $Na_V1.7$, $Na_V1.8$ and $Na_V1.9$ or TRPV1, are redistributed at the nerve endings during neuropathic or inflammatory conditions [32, 37, 41, 76]. Future investigation will determine whether increased DH Piezo2 is from redistributed in the central afferent endings or from upregulation of Piezo2 in the DH postsynaptic neurons ipsilateral to peripheral damage.

Peripheral non-neuronal cells play a key role in the induction and maintenance of persistent mechanical pain [49]. Here, we show that Piezo2 is expressed extensively in the PNS non-neuronal cells of various types. The skin acts as a complex sensory organ [49, 70, 100], and epidermal keratinocytes along with Merkel cells, Langerhans cells, and melanocytes express sensor proteins that regulate the neurocutaneous system and participate in nociception and mechanotransduction [49]. Non-neuronal skin Merkel cells express Piezo2, which is required for Merkel-cell mechanotransduction [22, 25, 87]. We detected Piezo2-IR in the skin epidermal Merkel cells and provide evidence that the epidermal melanocytes also express Piezo2 [49]. Skin melanocytes are dendritic cells and derived from skin Schwann cell precursors that origin from neural crest cells (NCC). Melanocytes form tight contacts with cutaneous nerves, respond to mechanical stretch [3, 15, 28, 35], and appear around

nerve fascicles after damage [60]. Pressure-sensing Merkel cells are thought of NCC origin [75], but new observations show that Merkel cells originate from epidermal progenitors but not NCCs [77]. Moreover, we found that PNS glia, including SGCs and SCs, express Piezo2. Piezo2-IR was colocalized to S100-positive dermal afferent nerve bundles and terminal fibers, suggesting that Piezo2 is expressed in the cutaneous SCs. Sensory neurons and SGCs/SCs, the two principal cell types of the PNS, interact intimately and are critical for normal PNS functions and pain pathogenesis during nerve injury and inflammation. Peripheral SCs can sense and transduce mechanical signals involving mechanosensation [8, 62], and the specialized cutaneous nociceptive nmSCs in skin determine the sensitivity threshold for mechanosensation [1]. Therefore, peripheral nerve SCs-Piezo2 may play hitherto unexplored roles in sensory processing and mechanotransduction; for instance, by regulating signaling within SCs initiated by mechanical stimulation [8, 12, 62].

We also detected extensive Piezo2 expression in rat brain neurons, consistent with a recent independent report showing Piezo2 expression in adult mouse brain neurons [80]. It is not wholly surprising to identify Piezo2 in brain since the *Piezo* gene was originally discovered in brain and dubbed as *Mib (*Membrane protein induced by Aβ) [65]; and study using brain neuronal analogue N2A cells discovers *Mib* as a mechanosensor and subsequently renamed as Piezo2 [17].

5. In conclusion, Piezo2 is widely expressed by neuronal and non-neuronal cells of the PNS and by neurons in the spinal cord and brain. Further study is needed to verify Piezo2 functions in these various cells. Overall, our results suggest that Piezo2 is not only involved in detection of external mechanical stimuli in the skin, but may also serve to detect internal mechanical cues in the nervous system or link to other unexplored intercellular and intracellular signaling pathways in the pain circuits [9]. Our findings provide additional sites for further investigation to fully understand the roles of Piezo2 in sensation and related to pain pathogenesis.

Supplementary Material

Refer to Web version on PubMed Central for supplementary material.

Acknowledgments

We thank Dr. Ardem Patapoutian for providing Piezo2 knockout (ko) mice (*Hoxb8Cre*/*Piezo2*$^{fl/fl}$). This research was supported by a grant from the Department of Veterans Affairs Rehabilitation Research and Development I01RX001940 (to QH), a National Institutes of Health grant R61NS116203 (to HY and QH), a National Institutes of Health grants NS108278 (to CLS), and an MCW NRC grant FP00016291 (to HY).

References

[1]. Abdo H, Calvo-Enrique L, Lopez JM, Song J, Zhang MD, Usoskin D, El Manira A, Adameyko I, Hjerling-Leffler J, Ernfors P. Specialized cutaneous Schwann cells initiate pain sensation. Science 2019;365(6454):695–699. [PubMed: 31416963]

[2]. Abraira VE, Kuehn ED, Chirila AM, Springel MW, Toliver AA, Zimmerman AL, Orefice LL, Boyle KA, Bai L, Song BJ, Bashista KA, O'Neill TG, Zhuo J, Tsan C, Hoynoski J, Rutlin M, Kus L, Niederkofler V, Watanabe M, Dymecki SM, Nelson SB, Heintz N, Hughes DI, Ginty DD.

The Cellular and Synaptic Architecture of the Mechanosensory Dorsal Horn. Cell 2017;168(1–2):295–310 e219. [PubMed: 28041852]

[3]. Adameyko I, Lallemend F, Aquino JB, Pereira JA, Topilko P, Muller T, Fritz N, Beljajeva A, Mochii M, Liste I, Usoskin D, Suter U, Birchmeier C, Ernfors P. Schwann cell precursors from nerve innervation are a cellular origin of melanocytes in skin. Cell 2009;139(2):366–379. [PubMed: 19837037]

[4]. Alamri A, Bron R, Brock JA, Ivanusic JJ. Transient receptor potential cation channel subfamily V member 1 expressing corneal sensory neurons can be subdivided into at least three subpopulations. Front Neuroanat 2015;9:71. [PubMed: 26106303]

[5]. Andersen ND, Srinivas S, Pinero G, Monje PV. A rapid and versatile method for the isolation, purification and cryogenic storage of Schwann cells from adult rodent nerves. Sci Rep 2016;6:31781. [PubMed: 27549422]

[6]. Anderson EO, Schneider ER, Bagriantsev SN. Piezo2 in Cutaneous and Proprioceptive Mechanotransduction in Vertebrates. Curr Top Membr 2017;79:197–217. [PubMed: 28728817]

[7]. Bagriantsev SN, Gracheva EO, Gallagher PG. Piezo proteins: regulators of mechanosensation and other cellular processes. J Biol Chem 2014;289(46):31673–31681. [PubMed: 25305018]

[8]. Belin S, Zuloaga KL, Poitelon Y. Influence of Mechanical Stimuli on Schwann Cell Biology. Front Cell Neurosci 2017;11:347. [PubMed: 29209171]

[9]. Borbiro I, Rohacs T. Regulation of Piezo Channels by Cellular Signaling Pathways. Curr Top Membr 2017;79:245–261. [PubMed: 28728819]

[10]. Bron R, Wood RJ, Brock JA, Ivanusic JJ. Piezo2 expression in corneal afferent neurons. J Comp Neurol 2014;522(13):2967–2979. [PubMed: 24549492]

[11]. Chamessian A, Young M, Qadri Y, Berta T, Ji RR, Van de Ven T. Transcriptional Profiling of Somatostatin Interneurons in the Spinal Dorsal Horn. Sci Rep 2018;8(1):6809. [PubMed: 29717160]

[12]. Chen Y, Ju L, Rushdi M, Ge C, Zhu C. Receptor-mediated cell mechanosensing. Mol Biol Cell 2017;28(23):3134–3155. [PubMed: 28954860]

[13]. Chesler AT, Szczot M, Bharucha-Goebel D, Ceko M, Donkervoort S, Laubacher C, Hayes LH, Alter K, Zampieri C, Stanley C, Innes AM, Mah JK, Grosmann CM, Bradley N, Nguyen D, Foley AR, Le Pichon CE, Bonnemann CG. The Role of PIEZO2 in Human Mechanosensation. N Engl J Med 2016;375(14):1355–1364. [PubMed: 27653382]

[14]. Chiu IM, Barrett LB, Williams EK, Strochlic DE, Lee S, Weyer AD, Lou S, Bryman GS, Roberson DP, Ghasemlou N, Piccoli C, Ahat E, Wang V, Cobos EJ, Stucky CL, Ma Q, Liberles SD, Woolf CJ. Transcriptional profiling at whole population and single cell levels reveals somatosensory neuron molecular diversity. Elife 2014;3.

[15]. Cichorek M, Wachulska M, Stasiewicz A, Tyminska A. Skin melanocytes: biology and development. Postepy Dermatol Alergol 2013;30(1):30–41. [PubMed: 24278043]

[16]. Corder G, Siegel A, Intondi AB, Zhang X, Zadina JE, Taylor BK. A novel method to quantify histochemical changes throughout the mediolateral axis of the substantia gelatinosa after spared nerve injury: characterization with TRPV1 and substance P. J Pain 2010;11(4):388–398. [PubMed: 20350706]

[17]. Coste B, Mathur J, Schmidt M, Earley TJ, Ranade S, Petrus MJ, Dubin AE, Patapoutian A. Piezo1 and Piezo2 are essential components of distinct mechanically activated cation channels. Science 2010;330(6000):55–60. [PubMed: 20813920]

[18]. Cox CD, Bavi N, Martinac B. Biophysical Principles of Ion-Channel-Mediated Mechanosensory Transduction. Cell Rep 2019;29(1):1–12. [PubMed: 31577940]

[19]. Dezso Z, Nikolsky Y, Sviridov E, Shi W, Serebriyskaya T, Dosymbekov D, Bugrim A, Rakhmatulin E, Brennan RJ, Guryanov A, Li K, Blake J, Samaha RR, Nikolskaya T. A comprehensive functional analysis of tissue specificity of human gene expression. BMC Biol 2008;6:49. [PubMed: 19014478]

[20]. Dubin AE, Patapoutian A. Nociceptors: the sensors of the pain pathway. J Clin Invest 2010;120(11):3760–3772. [PubMed: 21041958]

[21]. Dubin AE, Schmidt M, Mathur J, Petrus MJ, Xiao B, Coste B, Patapoutian A. Inflammatory signals enhance piezo2-mediated mechanosensitive currents. Cell Rep 2012;2(3):511–517. [PubMed: 22921401]

[22]. Feng J, Luo J, Yang P, Du J, Kim BS, Hu H. Piezo2 channel-Merkel cell signaling modulates the conversion of touch to itch. Science 2018;360(6388):530–533. [PubMed: 29724954]

[23]. Fischer G, Kostic S, Nakai H, Park F, Sapunar D, Yu H, Hogan Q. Direct injection into the dorsal root ganglion: technical, behavioral, and histological observations. J Neurosci Methods 2011;199(1):43–55. [PubMed: 21540055]

[24]. Fotiou E, Martin-Almedina S, Simpson MA, Lin S, Gordon K, Brice G, Atton G, Jeffery I, Rees DC, Mignot C, Vogt J, Homfray T, Snyder MP, Rockson SG, Jeffery S, Mortimer PS, Mansour S, Ostergaard P. Novel mutations in PIEZO1 cause an autosomal recessive generalized lymphatic dysplasia with non-immune hydrops fetalis. Nat Commun 2015;6:8085. [PubMed: 26333996]

[25]. Garcia-Mesa Y, Garcia-Piqueras J, Garcia B, Feito J, Cabo R, Cobo J, Vega JA, Garcia-Suarez O. Merkel cells and Meissner's corpuscles in human digital skin display Piezo2 immunoreactivity. J Anat 2017;231(6):978–989. [PubMed: 28905996]

[26]. George D, Ahrens P, Lambert S. Satellite glial cells represent a population of developmentally arrested Schwann cells. Glia 2018;66(7):1496–1506. [PubMed: 29520852]

[27]. Gregory NS, Harris AL, Robinson CR, Dougherty PM, Fuchs PN, Sluka KA. An overview of animal models of pain: disease models and outcome measures. J Pain 2013;14(11):1255–1269. [PubMed: 24035349]

[28]. Hara M, Toyoda M, Yaar M, Bhawan J, Avila EM, Penner IR, Gilchrest BA. Innervation of melanocytes in human skin. J Exp Med 1996;184(4):1385–1395. [PubMed: 8879211]

[29]. Haring M, Zeisel A, Hochgerner H, Rinwa P, Jakobsson JET, Lonnerberg P, La Manno G, Sharma N, Borgius L, Kiehn O, Lagerstrom MC, Linnarsson S, Ernfors P. Neuronal atlas of the dorsal horn defines its architecture and links sensory input to transcriptional cell types. Nat Neurosci 2018;21(6):869–880. [PubMed: 29686262]

[30]. Hill RZ, Bautista DM. Getting in Touch with Mechanical Pain Mechanisms. Trends Neurosci 2020;43(5):311–325. [PubMed: 32353335]

[31]. Jager SE, Pallesen LT, Richner M, Harley P, Hore Z, McMahon S, Denk F, Vaegter CB. Changes in the transcriptional fingerprint of satellite glial cells following peripheral nerve injury. Glia 2020;68(7):1375–1395. [PubMed: 32045043]

[32]. Ji RR, Samad TA, Jin SX, Schmoll R, Woolf CJ. p38 MAPK activation by NGF in primary sensory neurons after inflammation increases TRPV1 levels and maintains heat hyperalgesia. Neuron 2002;36(1):57–68. [PubMed: 12367506]

[33]. Jin P, Jan LY, Jan YN. Mechanosensitive Ion Channels: Structural Features Relevant to Mechanotransduction Mechanisms. Annu Rev Neurosci 2020;43:207–229. [PubMed: 32084327]

[34]. Kaplan A, Spiller KJ, Towne C, Kanning KC, Choe GT, Geber A, Akay T, Aebischer P, Henderson CE. Neuronal matrix metalloproteinase-9 is a determinant of selective neurodegeneration. Neuron 2014;81(2):333–348. [PubMed: 24462097]

[35]. Kippenberger S, Loitsch S, Muller J, Guschel M, Ramirez-Bosca A, Kaufmann R, Bernd A. Melanocytes respond to mechanical stretch by activation of mitogen-activated protein kinases (MAPK). Pigment Cell Res 2000;13(4):278–280. [PubMed: 10952396]

[36]. Koch SC, Acton D, Goulding M. Spinal Circuits for Touch, Pain, and Itch. Annu Rev Physiol 2018;80:189–217. [PubMed: 28961064]

[37]. Laedermann CJ, Cachemaille M, Kirschmann G, Pertin M, Gosselin RD, Chang I, Albesa M, Towne C, Schneider BL, Kellenberger S, Abriel H, Decosterd I. Dysregulation of voltage-gated sodium channels by ubiquitin ligase NEDD4–2 in neuropathic pain. J Clin Invest 2013;123(7):3002–3013. [PubMed: 23778145]

[38]. Lee W, Leddy HA, Chen Y, Lee SH, Zelenski NA, McNulty AL, Wu J, Beicker KN, Coles J, Zauscher S, Grandl J, Sachs F, Guilak F, Liedtke WB. Synergy between Piezo1 and Piezo2 channels confers high-strain mechanosensitivity to articular cartilage. Proc Natl Acad Sci U S A 2014;111(47):E5114–5122. [PubMed: 25385580]

[39]. Li L, Rutlin M, Abraira VE, Cassidy C, Kus L, Gong S, Jankowski MP, Luo W, Heintz N, Koerber HR, Woodbury CJ, Ginty DD. The functional organization of cutaneous low-threshold mechanosensory neurons. Cell 2011;147(7):1615–1627. [PubMed: 22196735]

[40]. Li Q, Lau A, Morris TJ, Guo L, Fordyce CB, Stanley EF. A syntaxin 1, Galpha(o), and N-type calcium channel complex at a presynaptic nerve terminal: analysis by quantitative immunocolocalization. J Neurosci 2004;24(16):4070–4081. [PubMed: 15102922]

[41]. Li Y, North RY, Rhines LD, Tatsui CE, Rao G, Edwards DD, Cassidy RM, Harrison DS, Johansson CA, Zhang H, Dougherty PM. DRG Voltage-Gated Sodium Channel 1.7 Is Upregulated in Paclitaxel-Induced Neuropathy in Rats and in Humans with Neuropathic Pain. J Neurosci 2018;38(5):1124–1136. [PubMed: 29255002]

[42]. Liu Z, Wang F, Fischer G, Hogan QH, Yu H. Peripheral nerve injury induces loss of nociceptive neuron-specific Galphai-interacting protein in neuropathic pain rat. Mol Pain 2016;12.

[43]. Maciel R, Bis DM, Rebelo AP, Saghira C, Zuchner S, Saporta MA. The human motor neuron axonal transcriptome is enriched for transcripts related to mitochondrial function and microtubule-based axonal transport. Exp Neurol 2018;307:155–163. [PubMed: 29935168]

[44]. Maksimovic S, Nakatani M, Baba Y, Nelson AM, Marshall KL, Wellnitz SA, Firozi P, Woo SH, Ranade S, Patapoutian A, Lumpkin EA. Epidermal Merkel cells are mechanosensory cells that tune mammalian touch receptors. Nature 2014;509(7502):617–621. [PubMed: 24717432]

[45]. Marques RF, Engler JB, Kuchler K, Jones RA, Lingner T, Salinas G, Gillingwater TH, Friese MA, Duncan KE. Motor neuron translatome reveals deregulation of SYNGR4 and PLEKHB1 in mutant TDP-43 amyotrophic lateral sclerosis models. Hum Mol Genet 2020;29(16):2647–2661. [PubMed: 32686835]

[46]. Marshall KL, Saade D, Ghitani N, Coombs AM, Szczot M, Keller J, Ogata T, Daou I, Stowers LT, Bonnemann CG, Chesler AT, Patapoutian A. PIEZO2 in sensory neurons and urothelial cells coordinates urination. Nature 2020;588(7837):290–295. [PubMed: 33057202]

[47]. Martinac B, Poole K. Mechanically activated ion channels. Int J Biochem Cell Biol 2018;97:104–107. [PubMed: 29471041]

[48]. Mikhailov N, Leskinen J, Fagerlund I, Poguzhelskaya E, Giniatullina R, Gafurov O, Malm T, Karjalainen T, Grohn O, Giniatullin R. Mechanosensitive meningeal nociception via Piezo channels: Implications for pulsatile pain in migraine? Neuropharmacology 2019;149:113–123. [PubMed: 30768945]

[49]. Moehring F, Halder P, Seal RP, Stucky CL. Uncovering the Cells and Circuits of Touch in Normal and Pathological Settings. Neuron 2018;100(2):349–360. [PubMed: 30359601]

[50]. Moehring F, Mikesell A, Sadler K, Stucky C. Piezo1 Mediates Keratinocyte Mechanotransduction. bioRvix 2020; doi: 10.1101/2020.07.19.211086.

[51]. Moroni M, Servin-Vences MR, Fleischer R, Sanchez-Carranza O, Lewin GR. Voltage gating of mechanosensitive PIEZO channels. Nat Commun 2018;9(1):1096. [PubMed: 29545531]

[52]. Murthy SE, Loud MC, Daou I, Marshall KL, Schwaller F, Kuhnemund J, Francisco AG, Keenan WT, Dubin AE, Lewin GR, Patapoutian A. The mechanosensitive ion channel Piezo2 mediates sensitivity to mechanical pain in mice. Sci Transl Med 2018;10(462).

[53]. Nonomura K, Woo SH, Chang RB, Gillich A, Qiu Z, Francisco AG, Ranade SS, Liberles SD, Patapoutian A. Piezo2 senses airway stretch and mediates lung inflation-induced apnoea. Nature 2017;541(7636):176–181. [PubMed: 28002412]

[54]. Parpaite T, Coste B. Piezo channels. Curr Biol 2017;27(7):R250–R252. [PubMed: 28376327]

[55]. Petersson S, Shubbar E, Enerback L, Enerback C. Expression patterns of S100 proteins in melanocytes and melanocytic lesions. Melanoma Res 2009;19(4):215–225. [PubMed: 19521263]

[56]. Ranade SS, Qiu Z, Woo SH, Hur SS, Murthy SE, Cahalan SM, Xu J, Mathur J, Bandell M, Coste B, Li YS, Chien S, Patapoutian A. Piezo1, a mechanically activated ion channel, is required for vascular development in mice. Proc Natl Acad Sci U S A 2014;111(28):10347–10352. [PubMed: 24958852]

[57]. Ranade SS, Syeda R, Patapoutian A. Mechanically Activated Ion Channels. Neuron 2015;87(6):1162–1179. [PubMed: 26402601]

[58]. Ranade SS, Woo SH, Dubin AE, Moshourab RA, Wetzel C, Petrus M, Mathur J, Begay V, Coste B, Mainquist J, Wilson AJ, Francisco AG, Reddy K, Qiu Z, Wood JN, Lewin GR, Patapoutian

A. Piezo2 is the major transducer of mechanical forces for touch sensation in mice. Nature 2014;516(7529):121–125. [PubMed: 25471886]

[59]. Rezaei N, Saghazadeh A. The Role of PIEZO2 in Human Mechanosensation. Acta Med Iran 2017;55(10):664. [PubMed: 29228535]

[60]. Rizvi TA, Huang Y, Sidani A, Atit R, Largaespada DA, Boissy RE, Ratner N. A novel cytokine pathway suppresses glial cell melanogenesis after injury to adult nerve. J Neurosci 2002;22(22):9831–9840. [PubMed: 12427839]

[61]. Roh J, Hwang SM, Lee SH, Lee K, Kim YH, Park CK. Functional Expression of Piezo1 in Dorsal Root Ganglion (DRG) Neurons. Int J Mol Sci 2020;21(11).

[62]. Rosso G, Young P, Shahin V. Implications of Schwann Cells Biomechanics and Mechanosensitivity for Peripheral Nervous System Physiology and Pathophysiology. Front Mol Neurosci 2017;10:345. [PubMed: 29118694]

[63]. Rutlin M, Ho CY, Abraira VE, Cassidy C, Bai L, Woodbury CJ, Ginty DD. The Cellular and Molecular Basis of Direction Selectivity of Adelta-LTMRs. Cell 2015;160(5):1027. [PubMed: 29698636]

[64]. Saitoh F, Araki T. Proteasomal degradation of glutamine synthetase regulates schwann cell differentiation. J Neurosci 2010;30(4):1204–1212. [PubMed: 20107048]

[65]. Satoh K, Hata M, Takahara S, Tsuzaki H, Yokota H, Akatsu H, Yamamoto T, Kosaka K, Yamada T. A novel membrane protein, encoded by the gene covering KIAA0233, is transcriptionally induced in senile plaque-associated astrocytes. Brain Res 2006;1108(1):19–27. [PubMed: 16854388]

[66]. Schneider ER, Anderson EO, Feketa VV, Mastrotto M, Nikolaev YA, Gracheva EO, Bagriantsev SN. A Cross-Species Analysis Reveals a General Role for Piezo2 in Mechanosensory Specialization of Trigeminal Ganglia from Tactile Specialist Birds. Cell Rep 2019;26(8):1979–1987 e1973. [PubMed: 30784581]

[67]. Shin SM, Cai Y, Itson-Zoske B, Qiu C, Hao X, Xiang H, Hogan QH, Yu H. Enhanced T-type calcium channel 3.2 activity in sensory neurons contributes to neuropathic-like pain of monosodium iodoacetate-induced knee osteoarthritis. Mol Pain 2020;16:1744806920963807. [PubMed: 33054557]

[68]. Shin SM, Itson-Zoske B, Cai Y, Qiu C, Pan B, Stucky CL, Hogan QH, Yu H. Satellite glial cells in sensory ganglia express functional transient receptor potential ankyrin 1 that is sensitized in neuropathic and inflammatory pain. Mol Pain 2020;16:1744806920925425. [PubMed: 32484015]

[69]. Shin SM, Wang F, Qiu C, Itson-Zoske B, Hogan QH, Yu H. Sigma-1 receptor activity in primary sensory neurons is a critical driver of neuropathic pain. Gene Ther 2020.

[70]. Shipton EA. Skin matters: identifying pain mechanisms and predicting treatment outcomes. Neurol Res Int 2013;2013:329364. [PubMed: 23766902]

[71]. Stucky CL, Lewin GR. Isolectin B(4)-positive and -negative nociceptors are functionally distinct. J Neurosci 1999;19(15):6497–6505. [PubMed: 10414978]

[72]. Sugisawa E, Takayama Y, Takemura N, Kondo T, Hatakeyama S, Kumagai Y, Sunagawa M, Tominaga M, Maruyama K. RNA Sensing by Gut Piezo1 Is Essential for Systemic Serotonin Synthesis. Cell 2020;182(3):609–624 e621. [PubMed: 32640190]

[73]. Szczot M, Liljencrantz J, Ghitani N, Barik A, Lam R, Thompson JH, Bharucha-Goebel D, Saade D, Necaise A, Donkervoort S, Foley AR, Gordon T, Case L, Bushnell MC, Bonnemann CG, Chesler AT. PIEZO2 mediates injury-induced tactile pain in mice and humans. Sci Transl Med 2018;10(462).

[74]. Szczot M, Pogorzala LA, Solinski HJ, Young L, Yee P, Le Pichon CE, Chesler AT, Hoon MA. Cell-Type-Specific Splicing of Piezo2 Regulates Mechanotransduction. Cell Rep 2017;21(10):2760–2771. [PubMed: 29212024]

[75]. Szeder V, Grim M, Halata Z, Sieber-Blum M. Neural crest origin of mammalian Merkel cells. Dev Biol 2003;253(2):258–263. [PubMed: 12645929]

[76]. Thakor DK, Lin A, Matsuka Y, Meyer EM, Ruangsri S, Nishimura I, Spigelman I. Increased peripheral nerve excitability and local NaV1.8 mRNA up-regulation in painful neuropathy. Mol Pain 2009;5:14. [PubMed: 19320998]

[77]. Van Keymeulen A, Mascre G, Youseff KK, Harel I, Michaux C, De Geest N, Szpalski C, Achouri Y, Bloch W, Hassan BA, Blanpain C. Epidermal progenitors give rise to Merkel cells during embryonic development and adult homeostasis. J Cell Biol 2009;187(1):91–100. [PubMed: 19786578]

[78]. Volkers L, Mechioukhi Y, Coste B. Piezo channels: from structure to function. Pflugers Arch 2015;467(1):95–99. [PubMed: 25037583]

[79]. Wang F, Xiang H, Fischer G, Liu Z, Dupont MJ, Hogan QH, Yu H. HMG-CoA synthase isoenzymes 1 and 2 localize to satellite glial cells in dorsal root ganglia and are differentially regulated by peripheral nerve injury. Brain Res 2016;1652:62–70. [PubMed: 27671501]

[80]. Wang J, Hamil O. Piezo2, a pressure sensitive channel is expressed in select neurons of the mouse brain: a putative mechanism for synchronizing neural networks by transducing intracranial pressure pulses. BioRxiv 2020; doi: 10.1101/2020.03.24.006452.

[81]. Wang J, La JH, Hamill OP. PIEZO1 Is Selectively Expressed in Small Diameter Mouse DRG Neurons Distinct From Neurons Strongly Expressing TRPV1. Front Mol Neurosci 2019;12:178. [PubMed: 31379500]

[82]. Wang L, Zhou H, Zhang M, Liu W, Deng T, Zhao Q, Li Y, Lei J, Li X, Xiao B. Structure and mechanogating of the mammalian tactile channel PIEZO2. Nature 2019;573(7773):225–229. [PubMed: 31435011]

[83]. Wercberger R, Braz J, Weinrich J, Basbaum A. Pain and itch processing by subpopulations of molecularly diverse spinal and trigeminal projection neurons. bioRxiv 2020; doi: 10.1101/2020.06.17.156091.

[84]. Witschi R, Johansson T, Morscher G, Scheurer L, Deschamps J, Zeilhofer HU. Hoxb8-Cre mice: A tool for brain-sparing conditional gene deletion. Genesis 2010;48(10):596–602. [PubMed: 20658520]

[85]. Won J, Vang H, Lee PR, Kim YH, Kim HW, Kang Y, Oh SB. Piezo2 Expression in Mechanosensitive Dental Primary Afferent Neurons. J Dent Res 2017;96(8):931–937. [PubMed: 28388364]

[86]. Woo SH, Lukacs V, de Nooij JC, Zaytseva D, Criddle CR, Francisco A, Jessell TM, Wilkinson KA, Patapoutian A. Piezo2 is the principal mechanotransduction channel for proprioception. Nat Neurosci 2015;18(12):1756–1762. [PubMed: 26551544]

[87]. Woo SH, Ranade S, Weyer AD, Dubin AE, Baba Y, Qiu Z, Petrus M, Miyamoto T, Reddy K, Lumpkin EA, Stucky CL, Patapoutian A. Piezo2 is required for Merkel-cell mechanotransduction. Nature 2014;509(7502):622–626. [PubMed: 24717433]

[88]. Wu HE, Gemes G, Zoga V, Kawano T, Hogan QH. Learned avoidance from noxious mechanical simulation but not threshold semmes weinstein filament stimulation after nerve injury in rats. J Pain 2010;11(3):280–286. [PubMed: 19945356]

[89]. Xiang H, Liu Z, Wang F, Xu H, Roberts C, Fischer G, Stucky C, Caron D, Pan B, Hogan Q, Yu H. Primary sensory neuron-specific interference of TRPV1 signaling by AAV-encoded TRPV1 peptide aptamer attenuates neuropathic pain. Mol Pain 2017;13:1744806917717040. [PubMed: 28604222]

[90]. Xiao R, Xu XZ. Mechanosensitive channels: in touch with Piezo. Curr Biol 2010;20(21):R936–938. [PubMed: 21056836]

[91]. Yanai I, Benjamin H, Shmoish M, Chalifa-Caspi V, Shklar M, Ophir R, Bar-Even A, Horn-Saban S, Safran M, Domany E, Lancet D, Shmueli O. Genome-wide midrange transcription profiles reveal expression level relationships in human tissue specification. Bioinformatics 2005;21(5):650–659. [PubMed: 15388519]

[92]. Yu H, Fischer G, Ferhatovic L, Fan F, Light AR, Weihrauch D, Sapunar D, Nakai H, Park F, Hogan QH. Intraganglionic AAV6 results in efficient and long-term gene transfer to peripheral sensory nervous system in adult rats. PLoS One 2013;8(4):e61266. [PubMed: 23613824]

[93]. Yu H, Fischer G, Jia G, Reiser J, Park F, Hogan QH. Lentiviral gene transfer into the dorsal root ganglion of adult rats. Mol Pain 2011;7:63. [PubMed: 21861915]

[94]. Yu H, Pan B, Weyer A, Wu HE, Meng J, Fischer G, Vilceanu D, Light AR, Stucky C, Rice FL, Hudmon A, Hogan Q. CaMKII Controls Whether Touch Is Painful. J Neurosci 2015;35(42):14086–14102. [PubMed: 26490852]

[95]. Yu H, Shin SM, Wang F, Xu H, Xiang H, Cai Y, Itson-Zoske B, Hogan QH. Transmembrane protein 100 is expressed in neurons and glia of dorsal root ganglia and is reduced after painful nerve injury. Pain Rep 2019;4(1):e703. [PubMed: 30801043]

[96]. Yu H, Shin SM, Xiang H, Chao D, Cai Y, Xu H, Khanna R, Pan B, Hogan QH. AAV-encoded CaV2.2 peptide aptamer CBD3A6K for primary sensory neuron-targeted treatment of established neuropathic pain. Gene Ther 2019;26(7–8):308–323. [PubMed: 31118475]

[97]. Zhang H, Wang Y. Identification of molecular pathway changes after spinal cord injury by microarray analysis. J Orthop Surg Res 2016;11(1):101. [PubMed: 27628653]

[98]. Zhang M, Wang Y, Geng J, Zhou S, Xiao B. Mechanically Activated Piezo Channels Mediate Touch and Suppress Acute Mechanical Pain Response in Mice. Cell Rep 2019;26(6):1419–1431 e1414. [PubMed: 30726728]

[99]. Zheng W, Nikolaev YA, Gracheva EO, Bagriantsev SN. Piezo2 integrates mechanical and thermal cues in vertebrate mechanoreceptors. Proc Natl Acad Sci U S A 2019;116(35):17547–17555. [PubMed: 31413193]

[100]. Zimmerman A, Bai L, Ginty DD. The gentle touch receptors of mammalian skin. Science 2014;346(6212):950–954. [PubMed: 25414303]

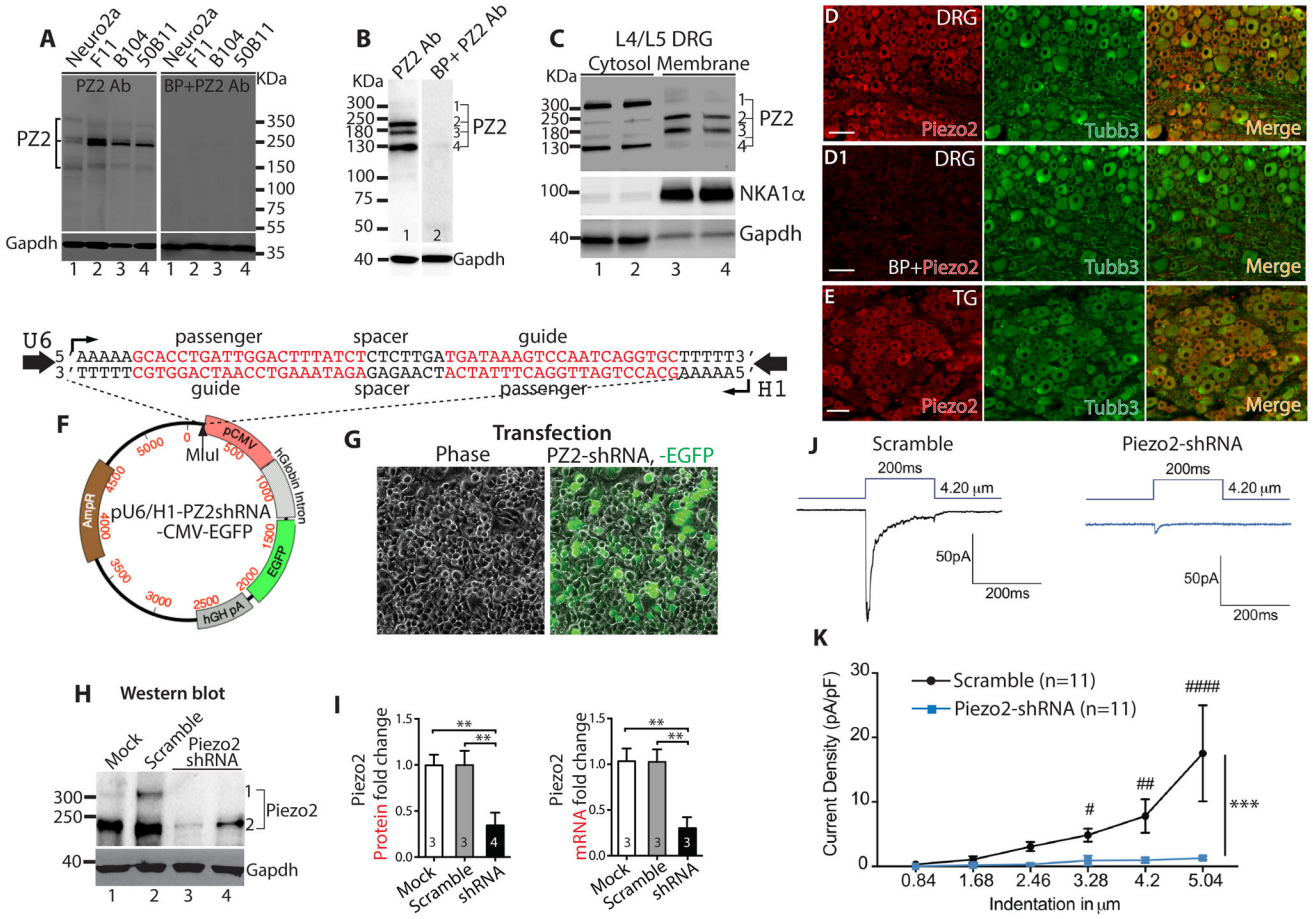

Figure 1. Specificity of Piezo2 (PZ2) antibody in detection of Piezo2 expression.

Several bands around 310–150KDa are detected by immunoblot (IB) in the lysates of neuronal cell lines, which are eliminated by preincubation with blocking peptide (BP) (**A**). In rat DRG lysate, the antibody detects several bands at approximately 310, 240, 180, and 130 KDa and they are eliminated by preincubation with BP (**B**). Piezo2 IB in the cytosolic and membrane fractions prepared from pooled L4/L5 DRG show that the antibody detected protein bands of ~240kDa and ~180kDa were more enriched in membranes while the protein bands with kDa at ~310 and ~130 were more enriched in cytosolic fractions (**C**). Representative images of double immunostaining (IS) of Piezo2 (red) and Tubb3 (green) on DRG sections reveal pan-neuronal Piezo2-IR (**D**) and preincubation with BP eliminated the staining (**D1**). Representative images of double-IS of Piezo2 (red) and Tubb3 (green) on trigeminal ganglia (TG) sections reveal pan-neuronal Piezo2-IR (**E**). Scale bars: 100 μm for all. Expression plasmid map (**F**) in which U6 and H1 promoters transcribe convergent apposing Piezo2-shRNA expression. The Piezo2-shRNA cassette (sequences shown on the top of plasmid map) is cloned into MluI site (pointed by arrowhead) of plasmid and named pU6/H1-Piezo2shRNA-CMV-EGFP (Piezo2-shRNA). Transfection of Piezo2-shRNA into N2A cells yielded 70–80% transfection rate (n=4) (**G**); Piezo2 protein in N2A lysates analyzed by IB using ProSci Piezo2 antibody: Lane 1, mock transfection; lane 2, transfection with scrambled RNA; lane 3–4, duplicate transfection using Piezo2-shRNA (**H**); Densitometry of IBs of fold change in Piezo2 protein (left) and qPCR (right) show

fold change in Piezo2 mRNA (**p<0.01, one-way ANOVA, Turkey *post-hoc* comparison) (**I**). Representative traces (**J**) and mean current density in response to mechanical force ramp (**K**) shows that Piezo2 knockdown significantly decreased mechanically-evoked rapid-adapt inward currents, compared to controls. ***p<0001; two-way ANOVA of main effects of groups with Bonferroni *post-hoc* comparison. $^{\#}$, $^{\#\#}$, and $^{\#\#\#}$ denote p<0.05, <0.01, and<0.001, respectively, between groups.

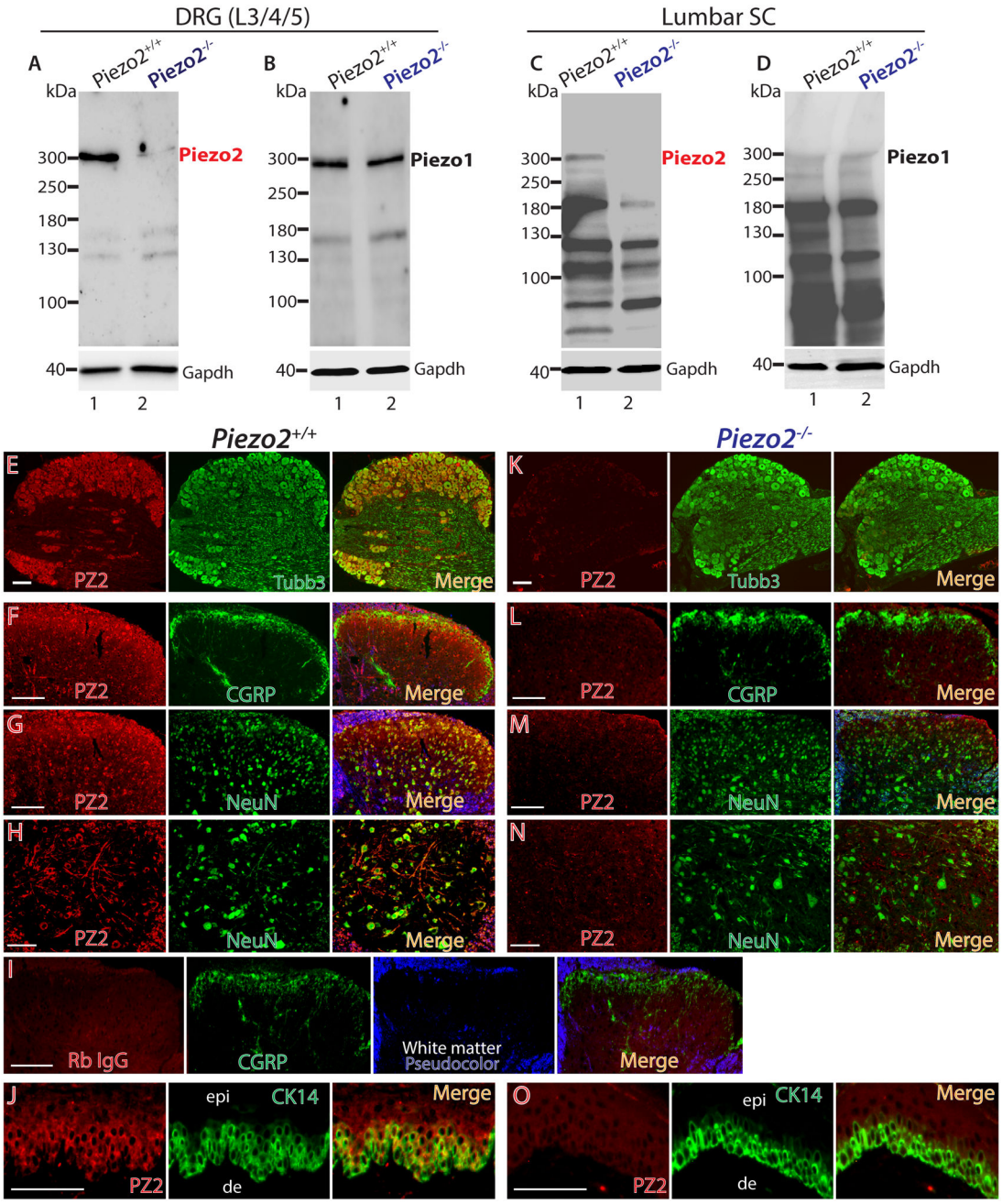

Figure 2. Validation of Piezo2 antibody in Piezo2 knockout (ko) mice.

DRG (equal 20μg protein loaded) and spinal cord (equal 50μg protein loaded) lysates were subjected to immunoblotting (IB) as shown in the representative IBs of Piezo2 and Piezo1. Piezo2 protein showing as a ~300kDa band in DRG (**A**) and lumbar spinal cord (**C**) lysates of wild-type mice was minimally detectable in the samples prepared from Piezo2-ko mice, while no apparent difference of Piezo1 protein levels in DRG (**B**) and spinal cord (**D**) was detectable between wild-type and Piezo2-ko samples. Representative IHC montage images revealed double immunostaining of Piezo2 (red) and Tubb3 (green), displaying colocalization (merged) in L5 DRG from wild-type mice (**E**) and Piezo2-ko mice

(*Hoxb8Cre*/*Piezo2*$^{fl/fl}$) (**K**). Representative montage images of lumbar spinal cord sections show Piezo2-IR (red) colabeled with CGRP (**F**, green) and NeuN (**G, H**) in wild-type mice, while Piezo2-IR in lumbar spinal cord sections is minimally detectable (**L**-**M**). No significant second antibody (donkey anti-rabbit Alexa-594 conjugated) staining is evident when Piezo2 antibody is replaced by rabbit IgG (1:100) (**I**). Representative montage images of hindpaw glabrous skin sections show Piezo2-IR (red) colabeled with cytokeratin (CK14, green) (**J**) in wild-type mice, while Piezo2-IR in hindpaw glabrous skin sections section is minimally detectable (**O**). Scale bars: 50 μm for all.

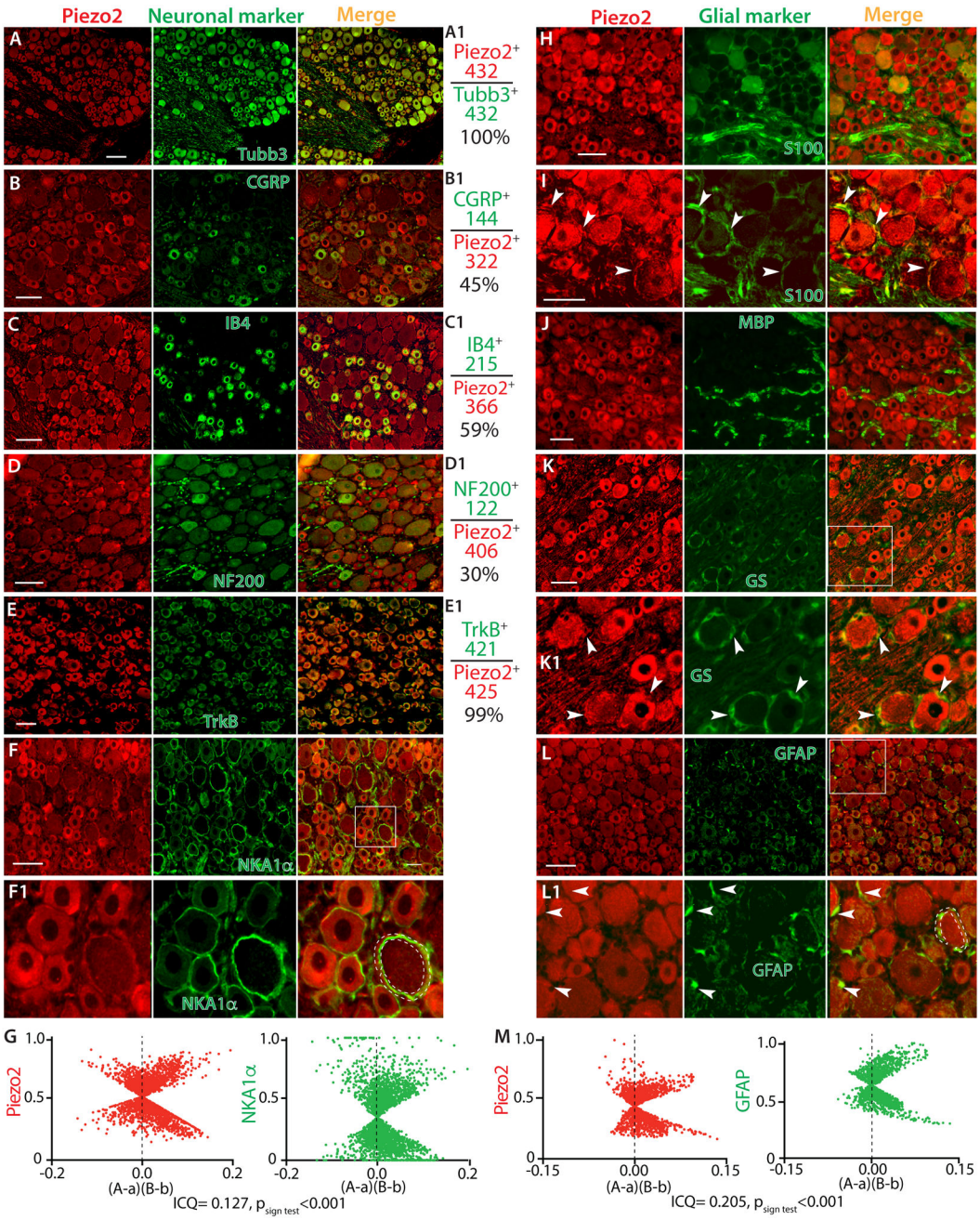

Figure 3. Double immunostaining (IS) of Piezo2 (PZ2) with a selection of neuronal and glial markers.

Representative montage images of DRG sections show Piezo2-IR (red) co-stained with a selection of DRG neuronal markers (green), including Tubb3 (**A**), IB4 (**B**), CGRP (**C**), NF200 (**D**), TrkB (**E**), and NKA1α (**F**) with the squared region shown at high magnification (**F1**). The panels in the right-side of **A**-**E** calculate the percentage of Piezo2-neurons overlaid to Tubb3-neurons (**A**1), as well as neurons positive for IB4 (**B1**), CGRP (**C1**), NF200 (**D1**), and TrkB (**E1**) overlaid to Piezo2-neurons. The numbers are the counted Piezo2-IR neurons (red) and marker-labeled neurons (green). ICA analyzes colocalization between Piezo2 and

NKA1α by an ImageJ 1.46r software plugin colocalization analysis module (**G**). Scatter plots for the region demarcated by the white dashed line in **F1** panel show data clustered along both positive and negative axes for both Piezo2 and NKA1α. "A" is the intensity of Piezo2 while "a" is the average of these values, and "B" is the intensity of NKA1a while "b" is the average of these values. For this region, the ICQ value is 0.127 ($P_{sign\ test}<0.001$), indicating partial immunocolocalization. Representative montage images show Piezo2 (red) with a selection of glial cell markers (green), including S100 (**H**, **I**), MBP (**J**), GS (**K**) with the squared region shown at high magnification (**K1**), and GFAP (**L**) with the squared region shown at high magnification (**L1**). White arrowheads in panel **I**, **K1**, and **L1** point to the immune-colabeled glial cells. ICA analysis for colocalization between Piezo2 and GFAP for the region demarcated by the white dashed line in **L1** panel show scattered plot data clustered along both positive and negative axes for both Piezo2 and GFAP. "A" is the intensity of Piezo2 while "a" is the average of these values, and "B" is the intensity of GFAP while "b" is the average of these values. For this region, the intensity correlation quotient (ICQ) value is 0.205 ($P_{sign\ test}<0.001$), indicating partial immunocolocalization (**M**). Scale bars: 50 μm for all.

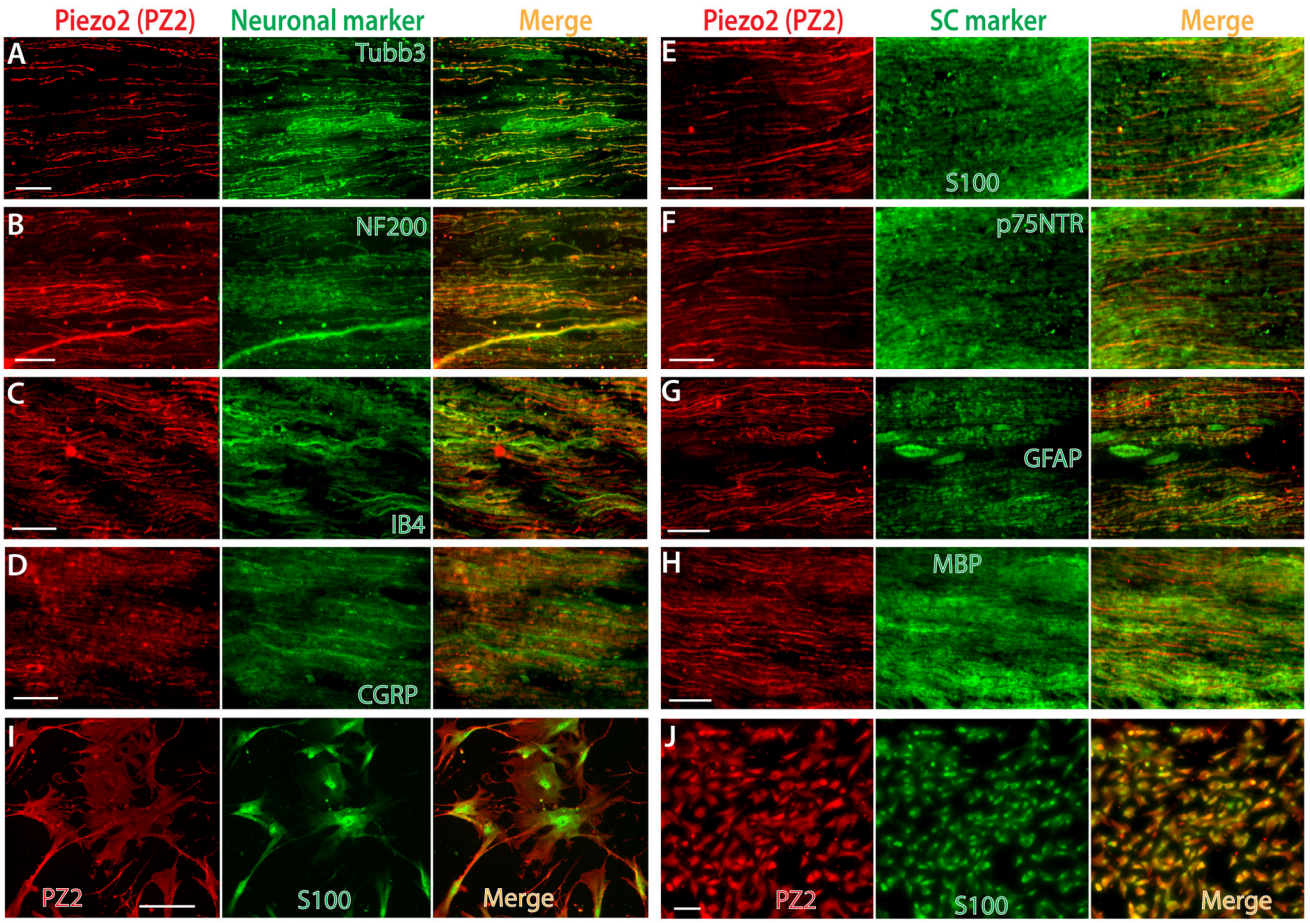

Figure 4. IHC delineation of Piezo2 (PZ2) axonal component and Schwann cell expression.

Representative montage images on sciatic nerve cryosections show double immunostaining (IS) of Piezo2 (red) with a selection of neuronal markers (green), including Tubb3 (**A**), NF200 (**B**), IB4 (**C**), and CGRP (**D**). Representative montage images on sciatic nerve cryosections show double-IS of Piezo2 (red) with glia markers (green), including S100 (**E**), p75NTR (**F**), GFAP (**G**), and MBP (**H**). Representative montage images on human Schwann cells (**I**) and isolated Schwann cells (**J**) from rat sciatic nerve show double-IS of Piezo2 (red) with S100 (green). Scale bars: 50 μm for all.

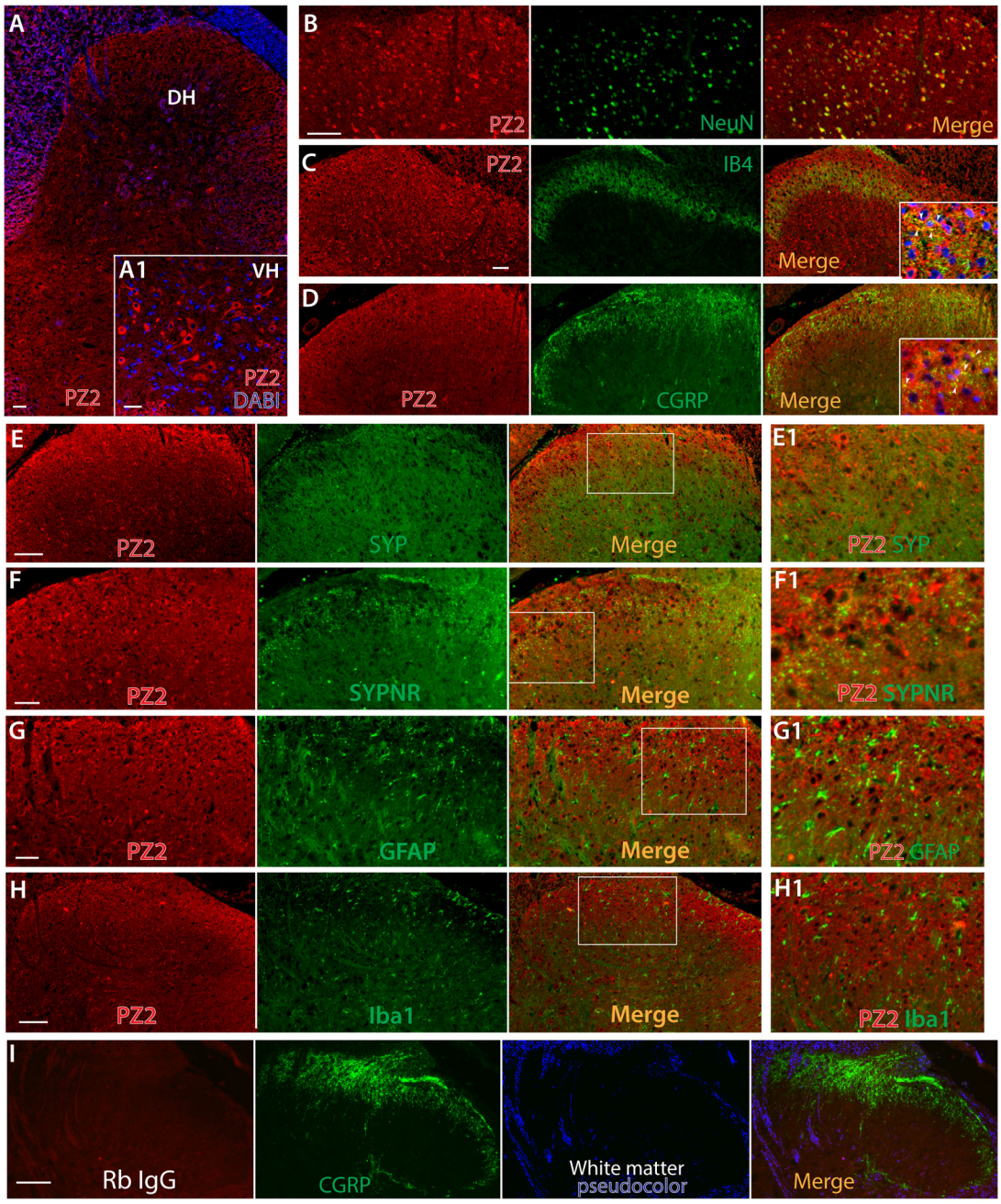

Figure 5. IHC delineation of Piezo2 (PZ2) expression in spinal cord.

Representative IHC image shows detection of Piezo2-IR (red) in the spinal cord neurons at all laminae (**A**), with grey matter pseudocolored in blue and a inset showing magnified image, counterstained with Hoechst (blue), of spinal ventral horn (**A1**). Representative montage images of double-IS on the DH regions reveal Piezo2-IR (red) with NeuN (green) (**B**) and a selection of dorsal horn presynaptic markers (green), including IB4 (**C**), CGRP (**D**), Syp (**E**), and Synpr (**F**), showing immunocolocalization (yellow) in the merged images. Insets in the merged images of panels **C** and **D** are higher magnifications of colabeling of Piezo2 (red) with IB4 or CGRP (green) with nuclear counterstained by

Hoechst (blue); arrowheads pointing to colocalization (yellow). Representative montage images show negative Piezo2 in GFAP-positive astrocytes (**G**) and Iba1-positive microglia (**H**) of spinal cord sections. The regions within the squares in panels **E**-**H** are shown at high magnification (**E1**-**H1**). There is no significant second antibody (donkey anti-rabbit Alexa-594 conjugated) staining when Piezo2 antibody is replaced by rabbit IgG (Rb IgG, 1:100) (**I**). Scale bars: 50 μm for all.

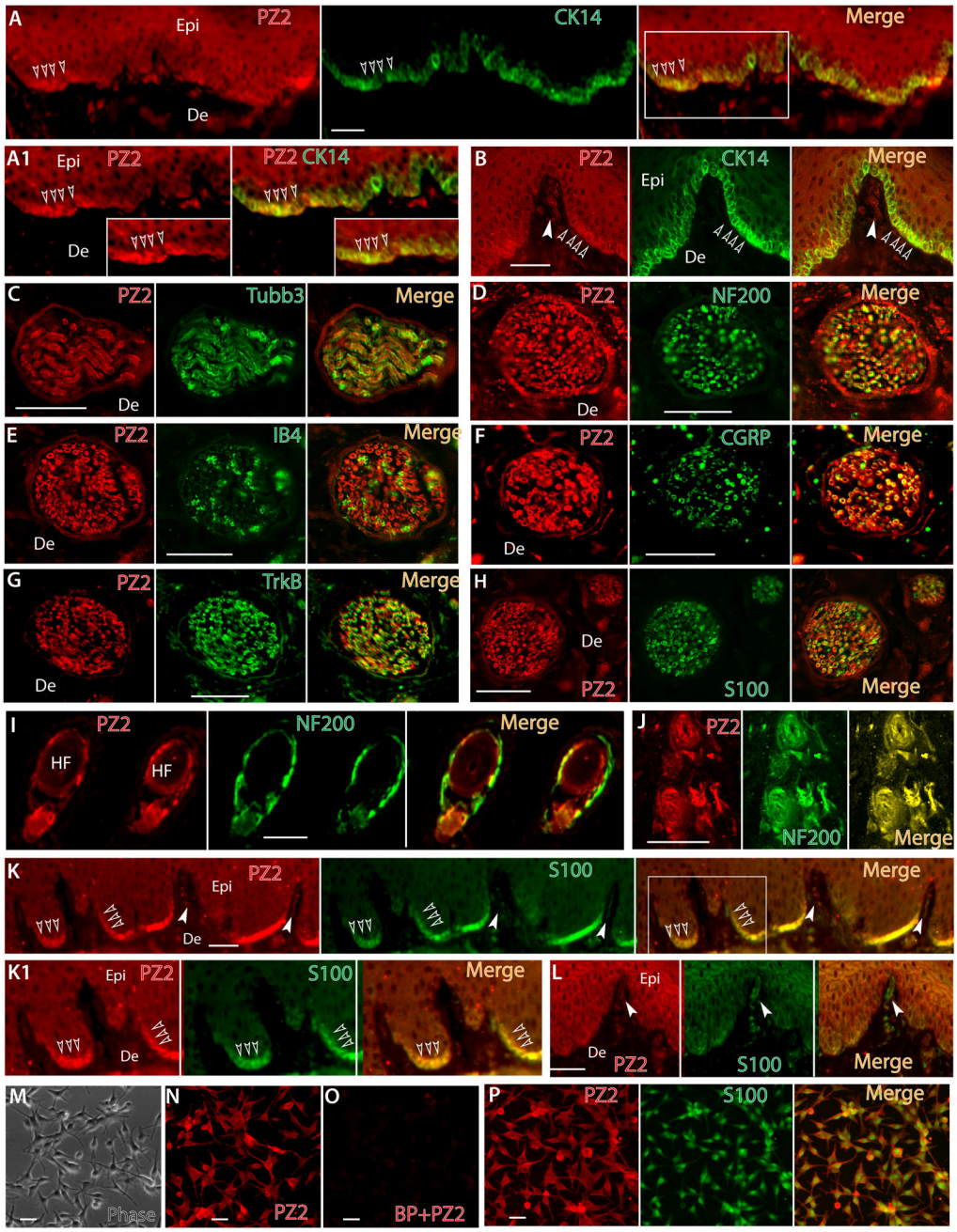

Figure 6. IHC delineation of Piezo2 (PZ2) expression in skin.

Representative montage images of hindpaw glabrous skin sections display double immunostaining (double-IS) of Piezo2 (red) with CK14 (green), a maker of epidermal basal layer keratinocytes and Merkel cells, showing colabeling (yellow, empty arrowheads) in the merged image (**A**) with the squared regions shown at high magnification (**A1**). Representative montage images reveal Piezo2-IR in Meissner's corpuscles (white arrowhead) and immunocolocalization with CK14-positive Merkel cells (empty arrowheads) (**B**). Representative montage images show immunocolocalization of Piezo2-IR with Tubb3 (**C**), NF200 (**D**), IB4 (**E**), CGRP (**F**), TrkB (**G**), and S100 (**H**) in the nerve bundles

within dermis, as well as lanceolate endings colabeled with NF200 around hair follicles (**I**, **J**). Representative montage images show immunocolocalization of Piezo2-IR with S100 in epidermal basal layer cells (**K**, empty arrowheads. White arrowheads point to Meissner's corpuscles), with the squared regions shown at high magnification (**K1**). Representative montage images show immunocolocalization of Piezo2-IR with S100 in Meissner's corpuscles (white arrowheads) (**L**). Human primary epidermal melanocytes (**M**) show Piezo2-IR (**N**) which is completely eliminated by blocking peptide preabsorption before ICC (**O**) and colabeled with S100 (**P**). Scale bars: 25 μm for all.

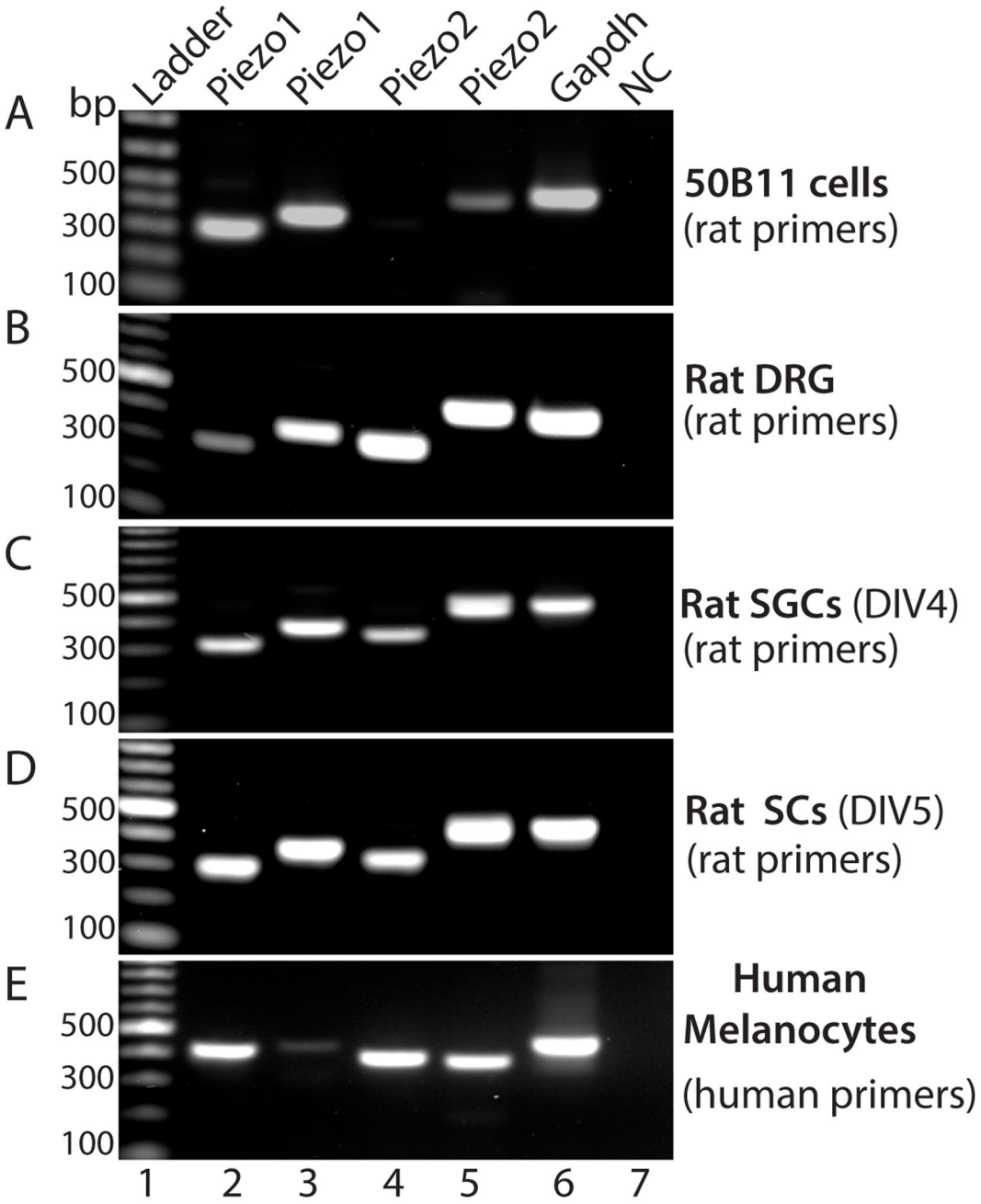

Figure 7. Validation of Piezos (2 and 1) expression by RT-PCR

RT-PCR shows amplification of Piezo1 and Piezo2 transcripts in rat 50B11 cells (**A**), rat DRG (**B**), rat primary cultured SGCs at day of in vitro 4 (DIV, **C**), and rat primary cultured Schwann cells at DIV5 (**D**) by two different primer pairs specific for amplification of rat Piezo1 and Piezo2 transcripts, as well as detection of Piezo1 and Piezo2 transcripts by two different primer pairs specific for human Piezo1 and 2 in human primary cultured melanocytes (**E**). Lane 1: ladder, lane 2–3: Piezo1 amplified by two piezo1 primer pairs (**A-D**, rat; **E**, human), lane 3–4: Piezo2 amplified by two piezo2 primer pairs (**A-D**, rat; **E**, human), lane 7: Gapdh, and lane 8: negative control.

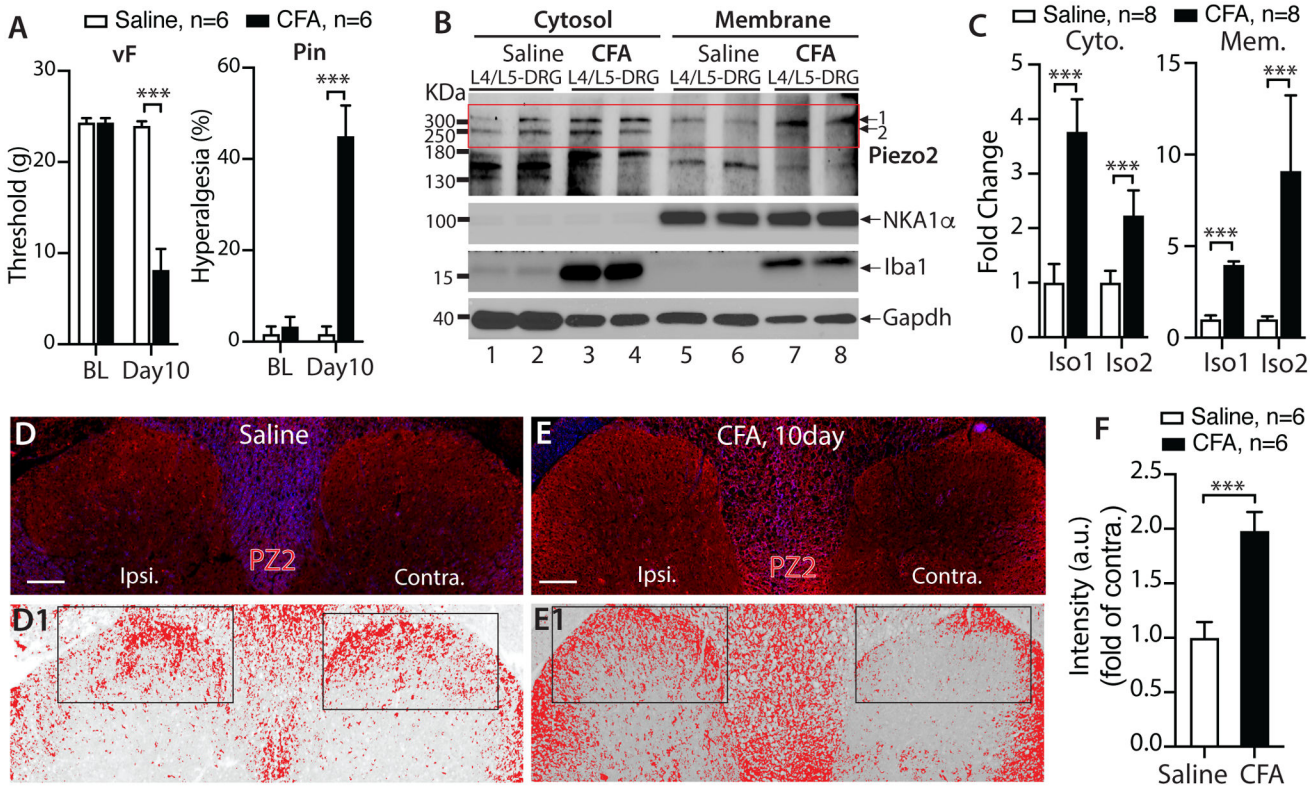

Figure 8. Aberrant Piezo2 (PZ2) expression in CFA-induced inflammatory pain

CFA rats developed mechanical allodynia (vF) and hyperalgesia (Pin) **A**); *** denotes $p<0.001$, unpaired, two-tailed Student's *t*-test for vF and Mann–Whitney test for Pin, compared between groups after CFA. NKA1α-deficient cytosolic fractions and NKA1α-enriched membrane fractions were extracted from the DRG (pooled L4/L5) at 10 days after CFA or saline injection, and subjected to immunoblotting (IB) as shown in the representative IBs of Piezo2, Iba1, NKA1α, and Gapdh of cytosol (**B**, left) and membrane fractions (**B**, right), respectively. The densitometry of canonical piezo2 (~310KDa, iso1) and putative iso2 (~250KDa) outlined by a rectangle were analyzed and summarized in bar charts (**C**); ***$p<0.001$, unpaired, two-tailed Student's *t*-test. Piezo2 intensities in DH of saline (**D**) and CFA (**E**) were inverted; the upper and lower threshold optical intensity of Piezo2-IR adjusted to encompass and match the IR that appears in red (**D1** and **E1**) with the rectangles positioned over laminae territory throughout the mediolateral axis on the contralateral (contra.) and ipsilateral (ipsi.) sides, and quantified as described in Method. Scale bars: 100 μm for all. The integrated density (product of area and density) calculated by use of ImageJ, and fold change (ratio of ipsi./contra.) summarized in the bar charts (**F**). *** denotes $p<0.001$ by two-tailed unpaired Student's *t*-test.

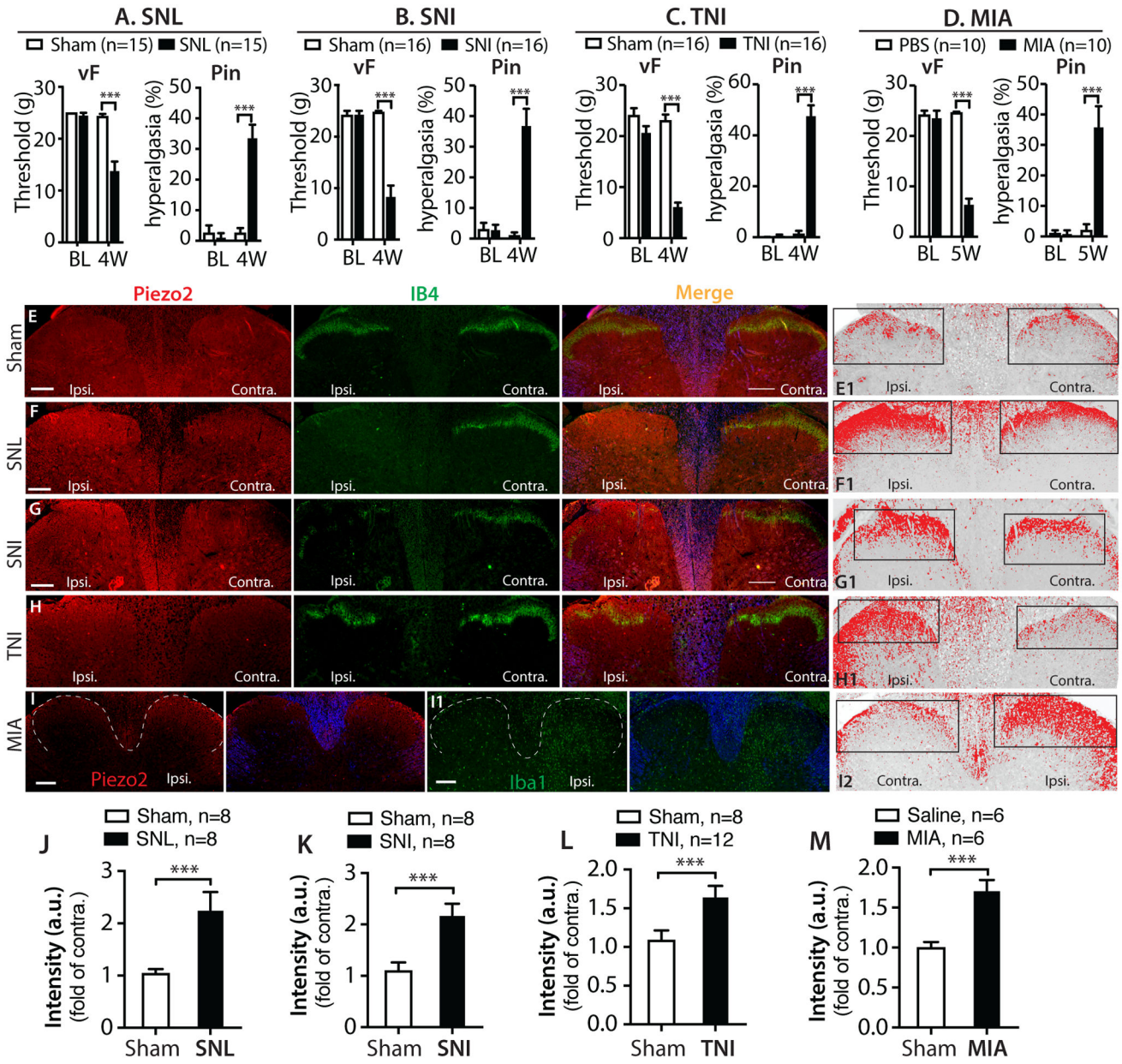

Figure 9. IHC characterization of Piezo2 (PZ2) expression in spinal DH in variety of rat pain models.

Bar charts summarize mechanical allodynia (vF) and hyperalgesia (Pin) that encompass various pain models in our previously published studies, as indicated (**A**-**D**). Representative IHC montage images on the DH show double immunostaining (IS) of Piezo2 (red) with IB4 (green) in control (**E**), SNL (**F**), SNI (**G**), and TNI (**H**) rats, and DH Piezo2-IR intensities from the presentative IHC images are inverted, and optical threshold adjusted encompass and match the IR that appears in red (**E1**-**H1**), respectively; and quantified as described in Method. The rectangles positioned over laminae territory throughout the mediolateral axis on the contralateral (contra.) and ipsilateral (ipsi.) DHs. The grey matters in the merged images are pseudocolored in blue. Representative IHC images of Piezo2 (red) (**I**) and Iba1

(**I1**) from two adjacent sections from MIA-OA rat display apparent increased Piezo2-IR in parallel with microgliosis at the ipsilateral side to MIA; white dash-lines outline the dorsal horns (left panels), and grey matters pseudocolored in blue (right panels), with image I of Piezo2 staining inverted and optical threshold adjusted (I2). Scale bars: 200μm for all. Quantitative comparison of DH Piezo2-IR intensity between ipsi. and contra. sides are analyzed by the Image J (see Methods and suppl. Fig.6), and the integrated intensity (product of area and density) calculated, and fold change (ratio of ipsi./contra.) presented as the bar charts in SNL (**J**), SNI (**K**), TNI (**L**), and MIA (**M**). *** denotes $p<0.001$ by two-tailed unpaired Student's *t*-test.

Table 1.

PCR and qPCR primers

Primer ID	Gene (species)	Forward primer sequence	Reverse primer sequence	Product size
RT-PCR				
rPZ1-F/R	*Piezo1* (Rat)	5'-CACTACTTCCACAGGCCGTT-3'	5'-AGACGTGAAGCTCGAGCAAA-3'	316bp
rPZ1-F1/R1	*Piezo1* (Rat)	5'-GCCGGCCATCTTGTTTGTTT-3'	5'-TGTCAATGTCGGGTCCAGTG-3'	376bp
rPZ2-F/R	*Piezo2* (Rat)	5'-GCAGTAGCATGTGCATTCCG-3'	5'-ATGGTCAGGCTCGCAATGAA-3'	350bp
rPZ2-F1/R1	*Piezo2* (Rat)	5'-GTATCACCATGCCAACCCCA-3'	5'-GGCGACCATGGCATGAATTC-3'	478bp
hPZ1-F/R	*PIEZO1* (human)	5'-GCGACACATAGGGGTCACAA-3'	5'-CCGAGTGCTGATGGGAAAGT-3'	424bp
hPZ1-F1/R1	*PIEZO1* (human)	5'-ACACCGAGGCTGATAACTGC-3'	5'-AGGGTGTAGAGCAACATGGC-3'	442bp
hZ2-F/R	*PIEZO2* (human)	5'-GCAGTAGCATGTGCATTCCG-3'	5'-CTGCTTCGTCTGTCACAGGT-3'	400bp
hZ2-F1/R1	*PIEZO2* (human)	5'-ACCTGTGACAGACGAAGCAG-3'	5'-AGCCAGCAGAACACAGAGAC-3'	391bp
Gapdh-F/R	*Gapdh* (rat/human)	5'-ACCACAGTCCATGCCATCAC-3'	5'-TCCACCACCCTGTTGCTGTA-3'	451bp
qPCR				
mPZ2-F/Rq	*Piezo2* (mouse)	5'-TCAGAACCAACCAAAGCAACG-3'	5'-TTGTAAGCAGGTGTGATGCGG-3'	151bp
Gapdh-F/Rq	*Gapdh* (mouse)	5'-CCCTTAAGAGGGATGCTGCC-3'	5'-TGTGAACGGATTTGGCCGTA-3'	123bp

Table 2.

Primary antibodies and IgG controls used in this study

Antibody[a]	Host	Supplier/Cat#[b]	Dilution
IB4		LF/I21413	1.0μg/ml
Piezo2	Rabbit polyclonal	Prosci/8613	1:100 (IHC), 1:1000 (Wb)
Piezo2	Rabbit polyclonal	Alomone/APC090 Cat#ab53852, RRID: AB_881796	1:100 (IHC), 1:1000 (Wb)
Piezo1	Rabbit polyclonal	Alomone/APC087	1:100 (IHC), 1:1000 (Wb)
CGRP	Mouse monoclonal	SCB/sc57053	1:600 (IHC)
GFAP	Rabbit polyclonal monoclonal	Dako/Z0334	1:1000 (IHC)
GFAP(GA5)	Mouse monoclonal	CS/3655	1:200 (IHC)
Tubb3	Mouse monoclonal monoclonal	SCB/sc80016	1:500 (IHC), 1:1000 (Wb)
NKA1α	Mouse monoclonal	SCB/sc514614	1:1000 (IHC)
TrkB	Mouse monoclonal	SCB/sc136990	1:500 (IHC)
GS	Mouse monoclonal	SCB/sc74430	1:800 (IHC)
S100	Mouse monoclonal	TF/MA5–12969	1:500 (IHC)
NF200	Mouse monoclonal	Sigma/N5389	1:1000 (IHC)
Syp	Mouse monoclonal	SCB/sc17750	1:200 (IHC)
Synpr	Mouse monoclonal	SCB/sc376761	1:200 (IHC)
CK14	Mouse monoclonal	SCB/sc53253	1:200 (IHC)
MBP	Mouse monoclonal	CS/41168	1:800 (IHC)
P75NTR	Mouse monoclonal	SCB/sc271708	1:100 (IHC)
Iba1	Rabbit polyclonal	Wako/019–19741	1:1000 (IHC)
Iba1	Mouse monoclonal	Sigma/ MABN92	1:200 (IHC)
GAPDH	Mouse monoclonal monoclonal	Sigma/SAB1403850	1:5000 (Wb)
IgG control	Mouse	LF/31903	1:100~400
IgG control	Rabbit	LF/MA5–16384	1:100~1000

[a]Antibody abbreviations IB4, Isolectin IB4; Piezo2 and 1, Piezo type mechanosensitive ion channel component 2 and 1; CGRP, calcitonin gene-related peptide; GFAP, Glial fibrillary acidic protein; Tubb3, β3-Tubulin; NKA1α, sodium/potassium ATPase 1α ; TrkB, tropomyosin receptor kinase B; GS, glutamine synthetase; NF200, neurofilament-200; Syp, synaptophysin; Synpr, synaptoporin; CK14, cytokeratin 14; MBP, myelin basic protein; P75NTR, neurotrophin receptor p75; GAPDH, glycolytic enzyme glyceraldehyde-3-phosphate dehydrogenase

[b]LF, Life Technologies, Carlsbad, CA; Alomone, Alomone Labs, Jerusalem, Israel; SCB, Santa Cruz Biotechnology, Santa Cruz, CA; CS: Cell signaling, Danvers, MA; Wako, Richmond, VA; Dako: Carpinteria, California; Sigma, Sigma-Aldrich, St Louis, MO